Competitive interactions between culturable bacteria are highly non-additive

Amichai Baichman-Kass, Tingting Song, Jonathan Friedman

Institute of Environmental Sciences, Hebrew University, Rehovot, Israel

Abstract

Microorganisms are found in diverse communities whose structure and function are determined by interspecific interactions. Just as single species seldom exist in isolation, communities as a whole are also constantly challenged and affected by external species. Though much work has been done on characterizing how individual species affect each other through pairwise interactions, the joint effects of multiple species on a single (focal) species, remain under explored. As such, it is still unclear how single species effects combine to a community-level effect on a species of interest. To explore this relationship, we assayed thousands of communities of two, three, and four bacterial species, measuring the effect of single, pairs of, and trios of 61 affecting species on six different focal species. We found that when multiple species each have a negative effect on a focal species, their joint effect is typically not given by the sum of the effects of individual affecting species. Rather, they are dominated by the strongest individual-species effect. Therefore, while joint effects of multiple species are often non-additive, they can still be derived from the effects of individual species, making it plausible to map complex interaction networks based on pairwise measurements. This finding is important for understanding the fate of species introduced into an occupied environment, and is relevant for applications in medicine and agriculture, such as probiotics and biocontrol agents, as well as for ecological questions surrounding migrating and invasive species.

Introduction

Scarce are the environments on Earth not colonized by bacteria. In addition to naturally playing important roles from driving biogeochemical cycles at the ecosystem level (Cavicchioli et al. 2019; Arrigo 2005; Falkowski, Fenchel, and Delong 2008) to supporting host health at the individual level (Berendsen, Pieterse, and Bakker 2012; Manor et al. 2020; Gilbert et al. 2018), bacteria have also been harnessed for countless biotechnological applications across industries such as food preservation (Motarjemi 2002), plant and animal health (Berendsen, Pieterse, and Bakker 2012; de Mello Júnior et al. 2021), biocontrol of pathogens (Köhl, Kolnaar, and Ravensberg 2019), as well as decomposition of toxic compounds, and production of valuable ones (Varjani, Gnansounou, and Pandey 2017; Ro et al. 2006; Fang and Smith, 2016; Mainka et al. 2021). In natural environments bacteria often form rich and complex communities, but understanding how these communities organize has proven difficult (Widder et al. 2016). Elucidating the rules that govern microbial ecology can both offer insight into larger ecological systems, and allow us to better manipulate and design microbial communities for desired functions.

The structure of microbial communities is determined by the interactions between the involved species (Konopka, Lindemann, and Fredrickson 2015; Barbier et al. 2018; Qian and Akçay 2020). In recent years, much effort has been put into measuring pairwise interactions of different species from, and in, different environments (Foster and Bell 2012; Vetsigian, Jajoo, and Kishony 2011; Kehe et al. 2021). But it is still unclear to what extent the joint effects of multiple species on a focal species of interest (e.g. a pathogen) can be inferred from pairwise measurements. Such inference may be challenging due to the presence of indirect interactions: the affecting species may alter each other's abundances (termed interaction chains), or may modify each other's effect on the focal species (termed interaction modification, or higher-order interactions) (Sanchez 2019; Wootton 2002).

Despite a strong theoretical foundation, empirical studies in recent years have shown conflicting results regarding the importance of higher order interactions and indirect effects (Levine et al. 2017). For some functions, such as degradation of complex molecules (Sanchez-Gorostiaga et al. 2019; Gralka et al. 2020) and antibiotic production (Tyc et al. 2014; Qi et al. 2021; Westhoff et al. 2021), clear evidence of such interactions has been found. Furthermore, in both empirical and theoretical studies, the presence or absence of an additional species has been shown to affect interactions, and even the outcome of invasion and coexistence in some systems (Mickalide and Kuehn 2019; Chang et al. 2022; Hsu et al. 2019). Additional theoretical work has shown that commonly used ecological models (i.e. generalized Lotka-Voltera) don't properly capture microbial community interactions, partially due to the nature of these interactions (chemically mediated as opposed to predator-prey) (Momeni, Xie, and Shou 2017). However other studies have shown that both structures of, and interactions within, larger communities can be accurately predicted from pairwise interactions alone, using variations of said models (Friedman, Higgins, and Gore 2017; Meroz et al. 2021; Guo and Boedicker 2016; Os et al. 2018). This being the case, how microbial interactions combine into the joint effect of multiple species on a single species of interest is still poorly understood.

In our research, we used high-throughput nanodroplet-based microfluidics to measure over 14,000 bacterial communities composed of subsets of a library of 61 soil and leaf isolates of which six were fluorescently labeled (Figure 1). We quantified the effect of individual species and the joint effects of species pairs and trios on the growth of six focal bacterial species and found that the effects of multiple species are dominated by the strongest single-species effect, and specifically that negative effects combine non-additively.

Results

We conducted high-throughput assays involving 61 affecting species and six different focal species to understand the effects of single species, pairs, and trios on the growth of a given (focal) species. The 61 affecting species included soil and leaf isolates as well as lab strains representing 19 genera from four phyla: Proteobacteria (n=14), Firmicutes (n=2), Bacteroidetes (n=2), and Actinobacteria (n=1) (full list in Supplementary File 1aand Data S1). The focal species were a subset of six of these species (all proteobacteria) that were transformed to constitutively express a fluorescent protein: (*Escherichia coli* [EC], *Ewingella americana* [EA], *Raoultella planticola* [RP]*, Buttiauxella izardii* [BI], *Citrobacter freundii* [CF], and *Pantoea agglomerans* [PA]) (see Materials and Methods). Except for EC which is a lab strain (*E. coli K-12* substr. *MG1655*), all focals were isolated from soil samples (Kehe et al. 2021). First, we characterized each species phylogenetically by performing Sanger sequencing of their 16S ribosomal RNA gene, and phenotypically by growing each species on each of 20 different carbon sources and 11 antibiotics. The species showed large variability in carbon utilization profiles with no species growing well on all carbon sources (Figure 1–figure supplement 3). There was also high variability in growth on antibiotics with 15 species showing little or no growth on any antibiotics, while 16 species showed resistance to at least 7 antibiotics (Figure 1–figure supplement 4).

We performed the interaction assays in the kChip microfluidics device (Kulesa et al. 2018; Kehe et al. 2019), allowing for extensive screening in parallel (see Materials and Methods, Figure 1–figure supplement 1). We measured the effects of 243 single species (18-52 for each of the 6 focal species), the joint effects of 5,357 species pairs (between 153 and 1464 for each of the 6 focal species), and the joint effects of 3,009 species trios (from a subset of 26 affecting species on one focal species). Cultures were normalized and mixed after pre-growth, such that the starting densities in the kChip were approximately 1:1 for all species in wells containing two droplets and two affecting species, but ratios varied in three droplet wells (see Materials and Methods, Figure 1–figure supplement 1,2). Interaction assays were carried out in minimal M9 media with 0.5% [w/v] glucose for 24 hours. The growth of the focal species was measured by fluorescence, and

effects were calculated as the log ratio of growth in coculture to growth in monoculture (see Materials and Methods, Figure 1D). Positive and negative effects are defined as a net increase or decrease in growth compared to the monoculture respectively, while affecting species with no observable effect (see Materials and Methods) were defined as neutral.

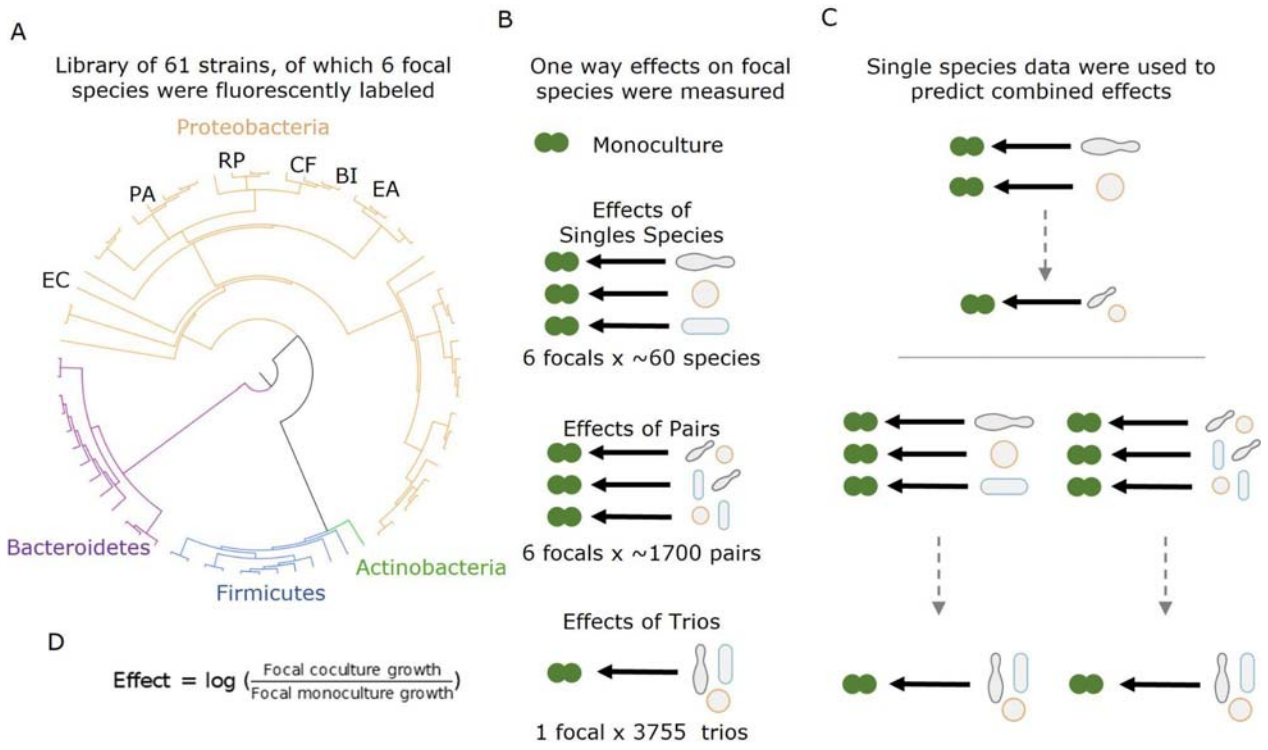

Figure 1: Measuring effects of 61 affecting species, and their pairs and trios on 6 focal species.

A) A library of 61 soil and leaf-associated bacterial strains was used in this experiment. All strains are from 4 orders: Proteobacteria (orange), Firmicutes (blue), Bacteroidetes (purple), and Actinobacteria (green) (full list in Supplementary File 1a*, Data S1). Six of the 61 species were labeled with GFP and used as 'focal' species whose growth was tested in the presence of the other isolates (affecting species). These strains are labeled on the phylogenetic tree (Escherichia coli [EC], Ewingella americana [EA], Raoultella planticola [RP], Buttiauxella izardii [BI], Citrobacter freundii [CF], and Pantoea agglomerans [PA], B) Each focal species was grown in monoculture, with (between 18-52) single affecting species, and (between* 153 and 1464*) pairs of affecting species. Additionally, E.coli was grown with* 3,009 *trios of affecting species. C) Effects of pairs and trios were then predicted using the effects of single species and single species and pairs respectively. Predictions were made using three different models: Additive, Mean, and Strongest (detailed in Results and Materials and Methods). D) Equation used for calculating the effect of an affecting species on the focal species.*

Joint effects of species pairs tend to be stronger than those of individual affecting species

We started our interaction assays by measuring the individual effects of single affecting species on each of the focal species (see Materials and Methods). Individual effects covered a wide range (median=-0.15, interquartile range=0.94) (Figure 2A), and positive effects (the focal species reaching a higher density in the presence of an affecting species than in monoculture) were common overall (32.9%, Figure 2B), in line with previous studies (Kehe et al. 2021). The distribution of effects varied based on the focal species, with *E. coli* and *B.izardii* showing the most negative (-2.83) and positive (+0.43) median effects, respectively (Figure 2D). Additionally, we found no affecting species that had strong effects across all focal species (Figure 2–Figure supplement 1).

The measured traits of individual species showed no consistent correlations with their effects on the focal species. In particular, the similarity of metabolic profile, resistance profile, or phylogeny between the focal and affecting species did not correlate strongly with the effect across focal species. Some traits showed little to no correlation for most focals (e.g. antibiotic resistance), while other traits were correlated with effect for a number focal species but not all (e.g. phylogenetic distance). Most of these correlations were not statistically significant (Figure 3–Figure supplement 1A).

After characterizing the individual effects of all single species, we assayed each pair of affecting species against the focal species. Overall, negative effects were significantly more prevalent in joint pair effects (77.1%) than in effects of individual species (60.5%) (p=1.3e-9, Fisher's exact test) (Figure 2B,C). The median effect on each focal was more negative by 0.28 on average, though the difference was not significant in all cases; additionally, focals with mostly positive single species interactions showed a small increase in median effect (Figure 2D). Despite this, the minimum and maximum effects for each focal species remained similar. As with the single affecting species, pairs' joint effects did not correlate well with species traits, with similarity between the two affecting species, or with their similarity to the focal species (Figure 3–Figure

supplement 1B). These results indicate that it may be challenging to connect the effects of single and pairs of species on a focal strain to a specific trait of the involved strains, using simple analysis.

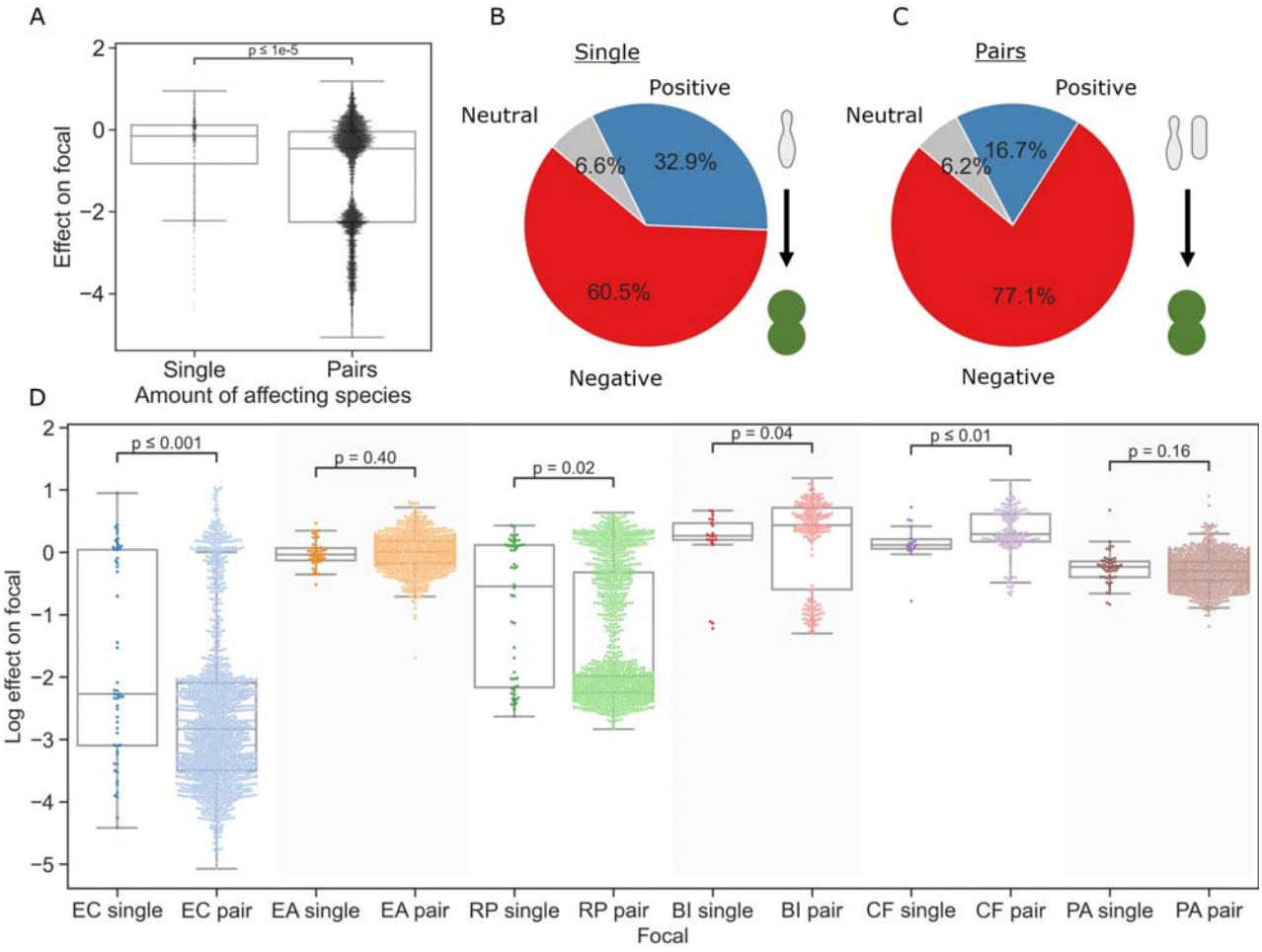

Figure 2: Pairs of affecting species have stronger effects than single species.

A) Distribution of the effects of single and pairs of affecting species on all focal species. Mann-Whitney-Wilcoxon test two-sided, p-value=1e-9. Dots show individual effects, solid lines represent the median, boxes represent the interquartile range, and whiskers are expanded to include values no further than 1.5X interquartile range. B,C) Distribution of qualitative effects of single and pairs of affecting species respectively on all focal species. D) Distribution of the effect of single and pairs of affecting species for each focal species individually. Dots represent individual measurements, solid lines represent the median, boxes represent the interquartile range, and whiskers are expanded to include values no further than 1.5X interquartile range. Mann-Whitney-Wilcoxon test two-sided tests were performed for each focal species, and p-values are shown on the graph.

Negative effects combine non-additively and joint effects are dominated by the stronger single species effect

Next, we examined how the effects of individual species relate to their joint effect. In particular, we were interested in finding a model that describes the effects of pairs, based on the data from single species effects. Based on previous studies' success in predicting community structure from pairwise interactions (Friedman, Higgins, and Gore 2017; Meroz et al. 2021; Guo and Boedicker 2016; Os et al. 2018), we posited that predicting how effects combine based solely on the effects of the single species should also be feasible. To do so, we considered three models: an additive effect model, a mean effect model, and a strongest effect model.

The additive effect model proposes that the effects of each species on the focal are the same whether they act individually or jointly. Therefore, the combined effect will be equal to the sum of the effects of each species on their own. This is equivalent to additivity of effects between antibiotics, which is common in the drug combinations field (Bollenbach 2015). The mean model represents a simple phenomenological model which assumes that the effects of different species will be diluted in the presence of a third species. By contrast, the strongest effect model posits that the species with the strongest effect dominates the effect of other affecting species, leaving the joint effect the maximum single effect, and not the sum or mean of single species effects.

When measured across all species and interaction types, we found that the model that best agrees with the measured effects is the strongest effect model (Figure 3B).Though supplementing the mean model with additional species information (i.e. carrying capacity) did improve the model accuracy, it was still less accurate than the strongest effect model (Figure 3–Figure supplement 2). The accuracy of the models and identity of the best fitting model varied across interaction types. The strongest effect model was the most accurate overall (nRMSE=0.46, 0.32, 0.16 for the additive, mean, and strongest models, correspondingly), and considerably more accurate when both species affected the focal negatively (nRMSE=0.65, 0.25, 0.16). The additive model was slightly more accurate when one effect was negative and the other positive (nRMSE=0.14, 0.43,

0.16). Overall, predictions when both effects were positive were less accurate, but here too the strongest model gave the most accurate predictions (nRMSE=0.81, 0.78, 0.69)(Figure 3C).

The distribution of errors further supported the strongest effect model (Figure 3B, Figure 3–Figure supplement 3B): When both single species effects were negative, the mean model was prone to underestimating the combined effect, due to the reduction of the stronger effect by taking into account the weaker effect; while contrastingly, the additive model overestimated effects due to the addition of the weaker effect to the stronger effect, which was more accurate on its own. We saw the opposite trend when both single species effects were positive, and no particular trend when there was one positive and negative effect. As with the effects themselves, model accuracy was not strongly correlated with any specific species trait (Figure 3–Figure supplement 4).

In regard to negative effects, support for the strongest model is also evident in how the difference in size of effect influences the model accuracy Figure 3–Figure supplement 3A). When effects are close to equal, the mean model is fairly accurate while the additive model does particularly poorly, as these effects would be calculated as twice the strongest effect. Contrastly, when one effect is much stronger than the other, the additive model is accurate since the addition of the weak effect is negligible, whereas the mean model underestimates the joint effects by taking into account the weaker effect.

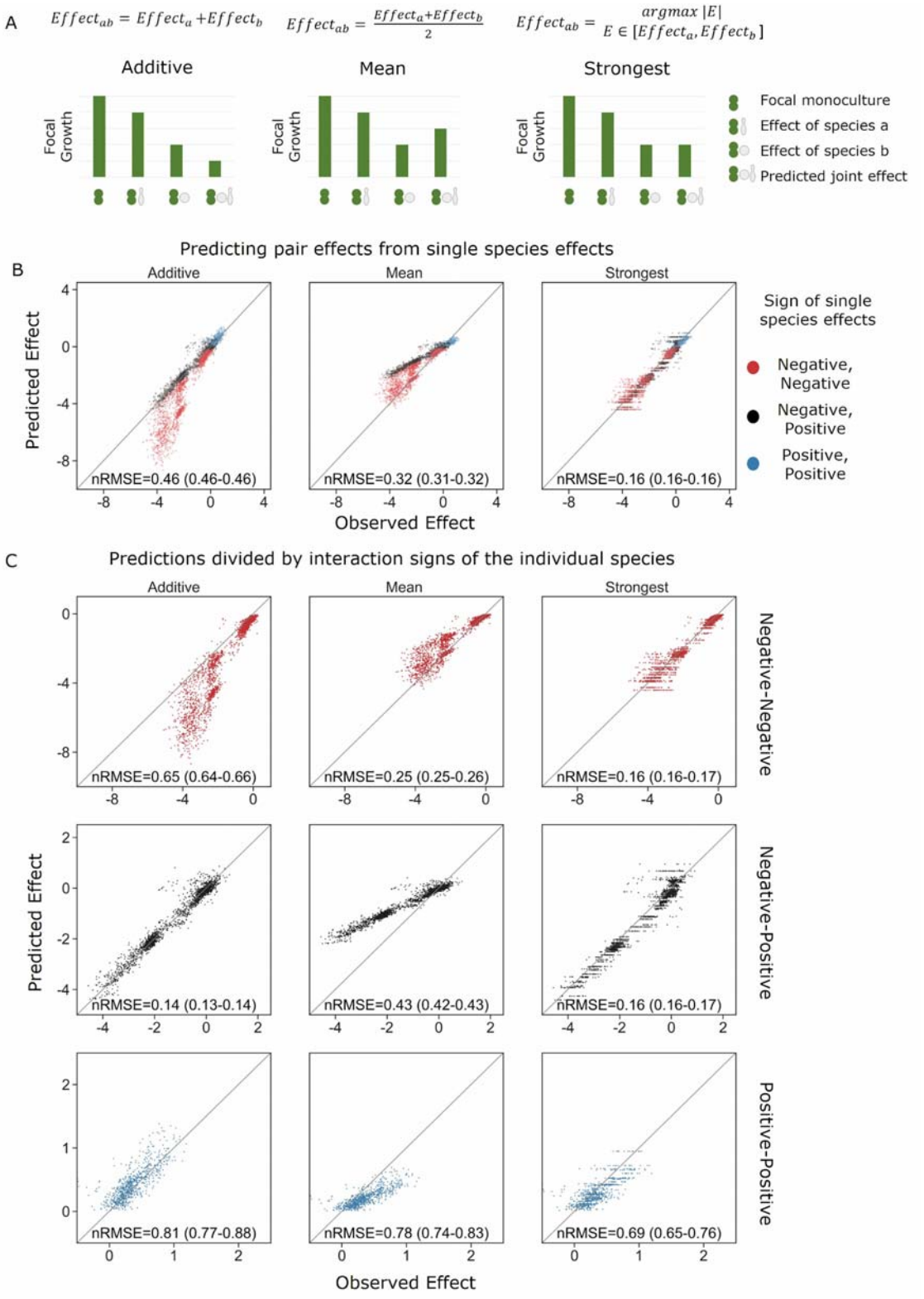

Figure 3: Strongest single species effect offers the most accurate model for the combined effect of two species. *A) Graphical representation for each model. The additive model assumes that the effects of each species will accumulate, indicating they are acting independently, and are unaffected by one another. The mean model assumes the combined effect will be an average of the two single species effects. The final model, strongest effect, assumes that whichever species had a stronger effect on its*

own will determine the joint effect when paired with an additional species. The y-axis represents the growth of the focal species in different conditions, and in these examples effects are negative. B) Comparison of predicted effects and the experimental data, with their respective root mean squared error normalized to the interquartile range of the observed data (nRMSE). nRMSE values are calculated from 1000 bootstrapped datasets, and represent the median and interquartile range in parentheses (see Materials and Methods). Each dot represents the joint effect of a pair of affecting species on a focal species. Colors indicate the signs of the measured effects of the individual affecting species. C) Similar to panel B, but data is stratified by interaction signs of the individual affecting species.

The strongest effect model is also the most accurate for larger communities

With this information in hand, we were interested to see if the same rules held up for larger communities. To this end, we screened trios of a subset (i.e. 26) of the affecting species against a single focal species (*E. coli*), and found similar trends to all those seen for pairs of affecting species. Similar to what was observed in the move from single species to pairs, effects were stronger (in this case more negative effects) in trios than in the pairs (Figure 4C). Additionally, as with joint pairs' effects, the strongest effect model was more accurate than the additive and mean models (nRMSE=2.65, 1.23, 0.63 for the additive, mean, and strongest models, correspondingly), which is consistent with the fact that the single species effects in this subset were predominantly negative. Similar distributions of error were seen as in the pairs' effects, but further exaggerated with the more extreme under and over estimation of the combined trios' effects by the mean and additive models respectively (Figure 4A).

We further explored the additive, mean, and strongest models in trios by basing the model on effects of the three pairs comprising each trio (i.e. joint effect of AB, AC, BC to predict effect of ABC), as opposed to only using single effect data (i.e. effect of A, B, C on their own) (Figure 4A,B). The effects of single species and pairs were measured again independently in this experiment (see Materials and Methods, Figure 1–figure supplement 1). The move to pairs-based predictions improved the accuracy for both the mean and strongest model, while further pushing the additive predictions away from the observed effects (Figure 4B). These data suggest that

even in the presence of additional species, the strongest single species effect still dominates the combined effect of a community.

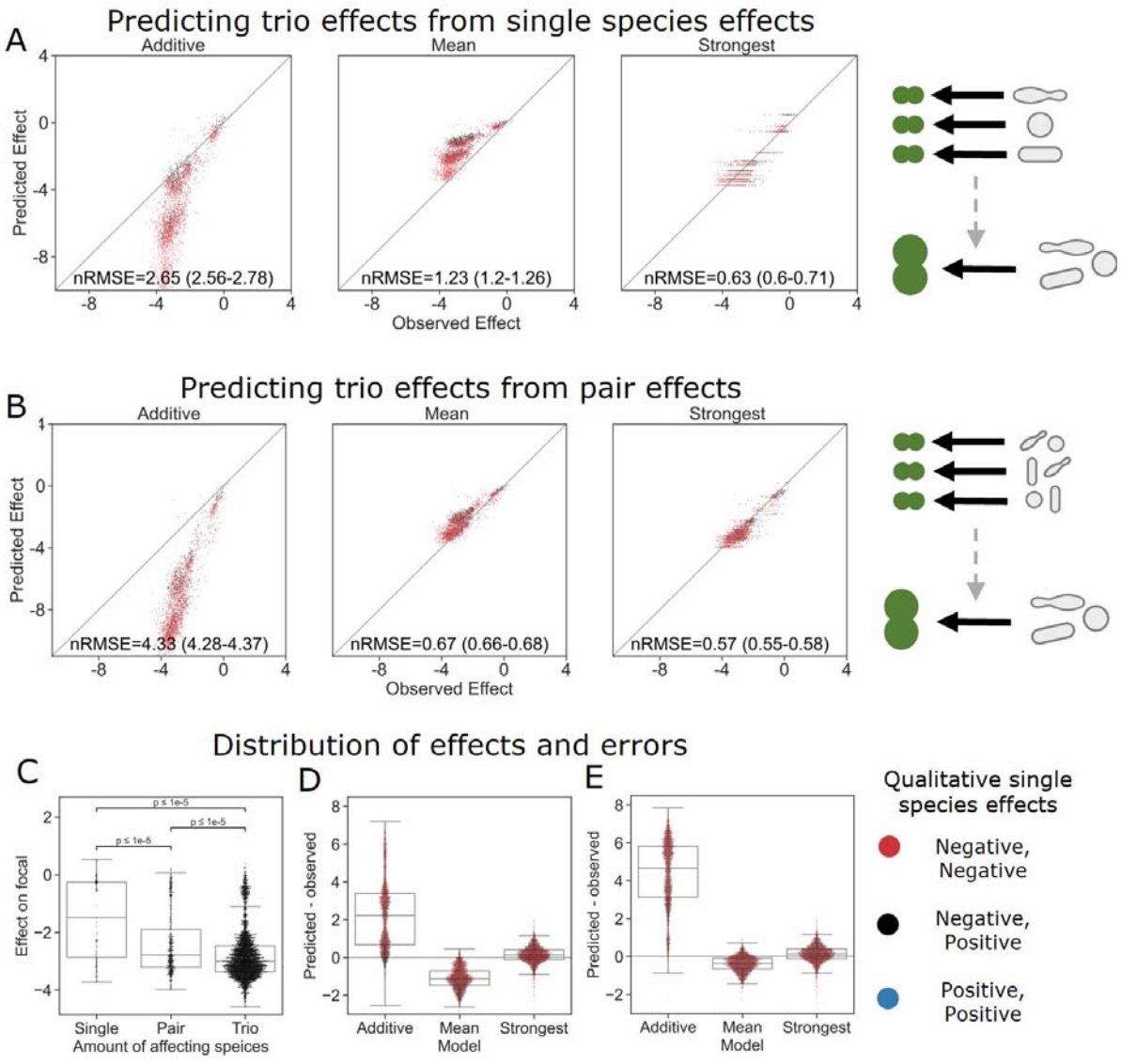

Figure 4: The strongest effect model is also the most accurate for trios.

A,B) Correlation between three different models for how A) single species effects and B) pairwise species effects combine into trio effects, and the experimental data. Root squared mean error normalized to the interquartile range. nRMSE values are calculated from 1000 datasets, and represent the median and interquartile range in parentheses (see Materials and Methods). C) Distribution of the effects of single, pairs and trios of affecting species on E. coli. All Mann-Whitney-Wilcoxon two-sided tests were significant, p values are shown on plot. Dots show individual effects, solid lines represent the median, boxes represent the interquartile range, and whiskers are expanded to include values no further than 1.5X interquartile range. D,E) Distribution of errors for each model based on D) single species data and E) pairs data. Dots

show individual effects, solid lines represent the median, boxes represent the interquartile range, and whiskers are expanded to include values no further than 1.5X interquartile range.

Discussion

By measuring thousands of simplified microbial communities, we quantified the effects of single species, pairs, and trios on multiple focal species. The most accurate model, overall and specifically when both single species effects were negative, was the strongest effect model. This is in stark contrast to models often used in antibiotic compound combinations, despite most effects being negative, where additivity is often the default model (Bollenbach 2015). The additive model performed well for mixed effects (i.e. one negative and one positive), but only slightly better than the strongest model, and poorly when both species had effects of the same sign. When both single species' effects were positive, the strongest model was also the best, though the difference was less pronounced and all models performed worse for these interactions. This may be due to the small effect size seen with positive effects, as when we limited negative and mixed effects to a similar range of effects strength, their accuracy dropped to similar values (Figure 3–Figure supplement 5). We posit that the difference in accuracy across species is affected mainly by the effect type dominating different focal species' interactions, rather than by inherent species traits (Figure 3–Figure supplement 6).

We phenotypically and genetically profiled all species, but did not find strong correlations between the measured traits, or similarity in traits, to the effect on the focal species. Though positive effects were common, making up about one third of the single species effects, they became less common as the number of community members increased, making up only 16% of the effects of species pairs. Furthermore, we found similar trends in the larger communities of 4 species (three affecting species and one focal), both that effects combined in a non-additive manner, being dominated by the strongest single species effect, and that effects became stronger in larger communities which is consistent with previous studies (Cook et al. 2006; van Elsas et al. 2012;

Jones et al. 2021; Piccardi, Vessman, and Mitri 2019; Gould et al. 2018; Palmer and Foster 2022).

The mechanistic basis underlying the joint effects of multiple species is still unclear. The additive model's accuracy for mixed effects may indicate that negative and positive effects act independently. For negative effects, it is difficult to identify a single biological mechanism that could explain why the strongest effect model agreed best with our experimental data. Intuitively, we assumed this could be explained by resource competition (i.e. an affecting species which consumes resources quickly would negatively affect the focal species, as well as the other affecting species). However, this explanation is not consistent with the fact that the affecting species' growth rate did not correlate well with their effect on some focal species (Figure 3–Figure supplement 1A). Secondly, we thought effects could be saturating (either biologically, or with regard to the detection limits in this experimental setup), but this would not explain why the model works for weaker effects. A hierarchical ranking, where each species affects all the species ranked below it could lead to the strongest affecting species affecting both the focal and the other affecting species, thus dominating their joint effects, but this does not coincide with the fact that we observed almost no single species or pairs with a strong effect across all focals (Figure 2–Figure supplement 1).

As we did not measure the abundance of all species in each community (only the focal), we cannot disentangle interaction modification (changes in per capita effect of specific species), from interaction chains (affecting the amount of an affecting species, and as such its effect on the focal), and further work is needed in order to pinpoint the exact mechanism(s) leading to the dominance of the strongest model for negative effects in our system. We also note that it is possible that the manner in which effects combine is affected by the mechanism of interaction; For instance, previous studies have shown that interference competition can combine additively, or even synergistically, results not seen in our work (Tyc et al. 2014; Westhoff et al. 2021).

Understanding how microbial communities assemble, and how large numbers of species interact is of both utmost importance and difficulty. Harnessing such information would open up a plethora of currently underutilized applications in food, medical, and agricultural industries. Specifically, understanding how the effects of multiple species on a single species combine is important for introduction of new species into a given environment. Our results suggest that when we want to affect a single focal species in a given environment (e.g. for biocontrol of a pathogen), introducing the species with the strongest effect on the focal would be sufficient to obtain the desired effect, as synergies were rare in our dataset. In cases where there are multiple strains of interest (e.g. probiotics), introducing multiple species may be beneficial since different affecting species typically have strong effects on different focals. Introducing combinations of species may allow for a more robust function, as the chances that one member of the community will have a strong effect on a resident species of interest is more likely.

Further work is needed in order to deepen our understanding of how multiple species affect each other and to see to what extent our findings continue to hold up in more diverse communities, other taxonomic groups, and more complex environments. Specifically, as we saw a decrease in prediction power from pairs to trios, exploring this model with more diverse communities is of particular interest. Additionally, nearly all of the effects in the 4 member communities were negative, and it is unclear how mixed and positive effect modeling is affected by higher diversity. Lastly, it is important to note that our focal species are all from the same order (Enterobacterales), which may also limit the purview of our findings. Nonetheless, our results suggest that community effects can be predicted from the strongest effect of a single species, greatly reducing the amount of information required to obtain accurate estimations, which can improve our ability to use a bottom-up approach for biotechnological applications, as well as answering fundamental ecology questions.

Materials and Methods

Strain isolation from soil samples

Soil (50 ml of soil, taken from a depth of ~30 cm) and leaf samples (multiple leaves from a single plant combined into a sterile 50 ml tube) were collected from various locations in the Faculty of Agriculture in Rehovot, Israel on multiple dates (See Data S1 file for more information). Each sample was diluted in phosphate-buffered saline (PBS) directly after collection (1 g of soil or one leaf in 10 ml of PBS) and vortexed for 5 minutes. 100 µl of multiple dilutions of this mixture (10^{-2}-10^{-5}) were seeded on different solid media [NB (0.5% [w/v] peptone, 0.3% [w/v] yeast extract, 1.5% [w/v] agar); 1% NB (0.005% [w/v] peptone, 0.003%[w/v] yeast extract, 1.5% agar); M9 minimal media (0.1 mM $CaCl_2$, 2mM $MgSO_4$, 1x [Enco-teknova] trace metals, 1% [w/v] glucose, 1x (Sigma) M9 Salts), additional plates were made with the same media containing various antibiotics (antibiotics and respective concentrations are listed in Supplementary File 1b S2) Plates were incubated at 30°C, and colonies were restreaked on NB without antibiotics until single isolates were stably obtained. Strains were selected on the basis of multiple criteria: growth of transferred colony in NB liquid medium (30°C), frozen glycerol stock revival in NB (OD_{600} > 0.1) (30°C), and subsequent growth on M9 minimal media + 1% (w/v) glucose (OD_{600} > 0.1) (30°C). Isolates were kept in single tubes as well as 96 well plates in 50% NB + 50% glycerol (glycerol stock were 60% and 80% for tubes and plates respectively for 30% and 40% final glycerol concentrations).

Strain identification and phylogenetic distance calculation

Each bacterial isolate was classified phylogenetically with its 16S rRNA gene sequence. The full 16S gene sequences (~1500 base pairs) were obtained via Sanger sequencing, and classified with a combination of RDP Classifier(Cole et al. 2014) and BLAST(Altschul et al. 1990) (List of strains in Supplementary File 1a, full phylogenetic data in Data S1 file). Phylogenetic distance was calculated in Geneious Prime software (version 2022.2.1, Biomatters Ltd). Sequences were aligned using MUSCLE alignment. Phylogenetic tree was built using the UPGMA method with no outgroup and a HKY genetic distance model. The pairwise phylogenetic distances between strains were calculated directly from the patristic distances of the phylogenetic tree.

Phenotypic profiling and distance calculation

Bacterial strains were seeded from -80 stock directly into 1 ml LB medium (1% [w/v] tryptone, 1% [w/v] NaCl, 0.5% [w/v] yeast extract) in 96 well plate, and grown overnight at 30°C at 900 RPM (on a Titramax 100 (Heidolph Instruments, Schwabach, Germany)). Cells were washed 3 times by centrifugation as 3600 rcf, removal of supernatant, and resuspension in M9 minimal media with no carbon. Cultures were then normalized to 0.01 OD_{600}. 20 µl of the normalized cultures were added to 180 µl of M9 minimal media either containing 1% [w/v] of one of 20 carbon sources (Supplementary File 1b) or M9 minimal media with 1% [w/v] glucose and one of 11 antibiotics (antibiotics and respective concentrations are listed in Supplementary File 1b). Plates were grown at 30°C for 48 hours without shaking. Cultures were homogenized by shaking (on a Titramax 100) for 90 seconds before measuring OD_{600}. Additionally, species were also grown in M9 minimal media (with the addition of 0.05% [w/v] BSA and 1% [w/v] glucose) with shaking (continuous double orbital shaking, 282 cpm) at 30°C, with OD measurements every 15 minutes, for 48 hours, to obtain growth kinetics (in Epoch and Synergy H1 microplate readers). Growth for carbon source experiments was normalized to the carbon source with the highest OD_{600} and antibiotic experiments were normalized to growth on M9 minimal media with glucose and no antibiotics. Euclidean distances of normalized values were measured for each species on carbon sources and antibiotics separately, and used to construct distance matrices. Growth kinetics (i.e. growth rate and carrying capacity) were not included in these profiles, but measured independently for correlation to effect size.

Droplet preparation and culturing

Bacterial strains were seeded from -80 stock directly into 1 ml LB medium (1% [w/v] tryptone, 1% [w/v] NaCl, 0.5% [w/v] yeast extract) in 96 well plate, and grown overnight at 30°C at 900 RPM (on a Titramax 100). Cells were washed 3 times by centrifugation as 3600 rcf for three minutes, removal of supernatant, and resuspension in M9 minimal media (with the addition of 0.05% [w/v] BSA and 1% [w/v] glucose). Affecting species cultures were then normalized to 0.04 OD_{600} and focal species cultures were to 0.02 OD_{600}. Affecting and focal species cultures were combined at

a ratio of 1:1 so that droplets contained a final concentration of 0.02 OD_{600} affecting species and 0.01 OD_{600} focal species. Each well contained droplets with the same focal species such that with this setup, in a well containing two droplets of different affecting species, the starting OD600 of each species is 0.01 (as each affecting species is diluted by the other droplet in which it is not contained, but the focal species is not). In wells with three droplets, the starting ratio of the focal to each affecting species (assuming different species in each droplet) was 3:2. When one of the droplets contains a monoculture of the focal or is empty, or more than one droplet contains the same affecting species, these ratios change (see Figure 1–figure supplement 1).

Droplets were produced on a Bio-Rad QX200 Droplet Generator as described by Kulesa *et al.*(Kulesa et al. 2018) Briefly, 20 µl input of combined cultures were emulsified into ~20,000 1 nl droplets in fluorocarbon oil (3M Novec 7500) stabilized with 2% (w/w) fluorosurfactant (RAN Biotech 008 FluoroSurfactant). 2.5 mM of fluorescent dyes (Thermo Fisher AlexaFluor™: 555 (A33080), 594 (A33082), 647 (A33084)) were added to culture for droplet imaging (See Kulesa et al.(Kulesa et al. 2018)). For each kChip loading, about 5000 droplets for each input (~60 affecting species + focal species, 2 focal species monocultures, 2 blank cultures) were generated, for a total of ~320,000 droplets. Droplets were generated together for 2 kChips (technical replicates), and then droplets were pooled separately for each chip. kChips were incubated at 30°C for 72 hours. Cultures were imaged at 24 hour intervals throughout the experiment. Data for analysis was taken from after 24 hours, as monoculture growth of the focals saturated by this point (Figure 1–figure supplement 5).

Fluorescence labeling and assays

Focal species were transformed with commercially available plasmid pMRE132 containing GFP2 by Kehe et al. 2021. Fluorescence has some caveats as a measurement for biomass, as fluorescent signal is not always directly proportional to biomass, expression levels can vary in different physiological states, and signal stability can differ between strains. Nonetheless, as described in Appendix 1, we show that effect sizes assayed using fluorescence and standard OD_{600} are well correlated (Appendix 1, Figure 1).

Data filtering and normalization

As the kChip genreates droplet combinations stochastically, the amount of replicates for each community is different, ranging from 1 to 285, with a mean of 19. All communities with less than 3 replicates were not used in the analysis. Additionally, isolates were only used with focals whose monocultures were at least five times larger than the isolates autofluorescence signal, allowing to measure effects of at least -1.5. Full datasets without autofluorescence filtering can be seen in Appendix 1, Figure 3. Importantly, affecting species autofluorescence would weaken measured negative effects, and would not systematically generate artifacts that support the strongest effect model. Normalization was performed by subtracting the starting value for each individual well from the additional time points.

Calculating effect size

To measure the effect of each affecting species on a given focal species, the log of the ratio of focal species yield in coculture (median of coculture replicates) to monoculture (median of monoculture replicates) was calculated:

$$Effect_i = log(\frac{Median\ growth\ of\ focal\ in\ coculture\ with\ species\ i}{Median\ growth\ of\ focal\ in\ monoculture}).$$

Coculture data was collected from wells with different starting concentrations in both the two-droplet experiments (i.e. one mixed droplet and one focal monoculture) and three-droplet experiments (i.e. two droplets of affecting species A and one droplet of affecting species B and vice versa, or one of each in addition to a blank droplet) (Figure 1–figure supplement 1). Our data showed that the different initial fractions did not influence the effect on the focal species (Figure 1–Figure supplement 2). The standard error was calculated via bootstrapping, 100 calculations of the resampled median coculture divided by resampled median monoculture. Effects where the standard deviation was larger than the absolute value of the effect were classified as neutral.

Calculating predictions for different models and their accuracy

The additive model assumes that the effects of each species will accumulate, and is the combined effect is the sum of effects, calculated as:

$$Effect_{(1\ldots n)} = Effect_1 + \ldots + Effect_n.$$

The mean model assumes the combined effect will be an average of the two single species effects, and is calculated as:

$$Effect_{(1\ldots n)} = \frac{Effect_1 + \ldots + Effect_n}{n}.$$

The OD-weighted mean model weighs the mean of effects by the affecting species' maximum OD_{600} in the growth curves experient and is calculated as:

$$Effect_{(1\ldots n)} = \frac{Effect_1 * max_{OD_{600}1} + \ldots + Effect_n * max_{OD_{600}n}}{max_{OD_{600}1} + \ldots + * max_{OD_{600}n}}.$$

The strongest effect model assumes that whichever species had a stronger effect on its own will determine the joint effect when paired with an additional species. It is calculated as:

$$Effect_{1\ldots n} = \underset{E \in [Effect_1, \ldots, Effect_n]}{argmax} |E|,$$

returning the effect with the largest absolute value (e.g. if two single species' effects are -3 and +1, the model will predict that their joint effect is -3).

Root mean square error measuring the accuracy of each model was normalized to the interquartile range for each dataset. Normalized root mean square error median and interquartile ranges were calculated via bootstrapping. The dataset from each focal was sampled 1000 times with replacement. Sampling was done for individual effect measurements (specific wells), and median effect sizes for species, pairs, and trios were recalculated from these sampled datasets. The sampled datasets from each focal were assembled into 'full' datasets (containing all focals) from which nRMSEs were calculated. The median and interquartile range of the normalized root mean square errors were calculated from the 1000 sampled datasets' values.

Acknowledgements

We thank Jared Kehe and Anthony Ortiz for helping set up the kChip system in our lab, as well as Meilin Zhu, Megan Tse, Julie Chen and Paul Blainey for continued correspondence and technical support. Alfonso Pérez Escudero, and members of the Friedman lab for helpful discussions. Nadav Kashtan for constructive comments on the manuscript. Eddie Cytryn for generously providing bacterial strains used in this study. Lastly, Yael Sorokin for technical assistance. This research was supported by the United States – Israel Binational Science Foundation (grant no. 2017179).

Figure supplement legends

Figure 1–figure supplement 1: **Species in each droplet and well in kChip experiments**
Droplets contained one of three different types of samples: 1) focal monoculture, containing only the focal species, 2) coculture of focal species and a single affecting species at an optical densities ratio of 2:1, 3) Blank samples, with media but no bacterial cells. Based on which two or three droplets (depending on the experimental setup) each well contained either a focal monoculture, one, two or three, affecting species. Similar communities started at different initial densities based on how many monoculture or blank droplets were in the well, but as shown in Figure 1–Figure supplement 2, initial densities did not influence the effect on the focal. Ratios of focal species to Affecting species 1 and 2 are detailed for different well setups.

Figure 1–Figure supplement 2: **Effects on focal species are independent of initial species' density**
Correlation between different ratios of initial optical density in each well. A) Different ratios of focal to affecting species based on whether there were two droplets containing the affecting species or one and one focal monoculture droplet- nRMSE=0.22 B) Different ratios of focal to affecting species based on whether there were three droplets containing the affecting species or one and two focal monoculture droplets- nRMSE=0.16. C) Different ratios of affecting species based on whether there were two droplets containing affecting species A and one droplet containing affecting species B or vice versa- nRMSE=0.33.

Figure 1–figure supplement 3: **Carbon source utilization profiles for bacterial strains**
Each strain's yield on 20 different carbon sources, assayed after 48 hours. Growth values are calculated as mean OD_{600} measurement from 3 replicates, and were background-subtracted (media with no bacteria).

Figure 1–figure supplement 4: **Antibiotic resistance profiles for bacterial strains**
Each strain's ability to grow on 11 different antibiotics, after 48 hours. Growth values are calculated as mean OD_{600} measurement from 3 replicates, and were background-subtracted (media with no bacteria).

Figure 1–figure supplement 5: **Growth dynamics of focal species in monoculture**
Growth in kChip of each focal strain in monoculture over 72 hours. Growth is measured by fluorescent signal and each well is normalized to the value at the beginning of the experiment (all signals at time zero are equal to one). The solid line represents the mean, and the shaded area the 95% confidence interval.

Figure 2–Figure supplement 1: **Minimal effect of single strains and pairs across multiple focals**
Distributions of the weakest effect of each individual species and pairs measured as the percentile within the distributions of effects for a single focal species (for affecting species that were measured against three or more focal species). For each species or pair, the minimal value from all focals was taken to generate the above distributions. Sign was not regarded in this calculation, only strength of the effect. Dots represent individual measurements, solid lines represent the

median, boxes represent the interquartile range, and whiskers are expanded to include values no further than 1.5X interquartile range. Mann-Whitney-Wilcoxon test two-sided tests were performed,and p-value is shown on the graph.

Figure 3–Figure supplement 1: **Correlation between affecting species traits and effect on focal**

Spearman correlation value for traits of A) single species, and B) pairs and effect on species separated for each focal species individually. Correlations with p-values below 0.05 are highlighted with a black frame. The growth rate, and maximum OD shown in panel A were measured only in M9 glucose, similar to conditions used in the interaction assays. See Materials and Methods for calculations of phenotypic and phylogenetic distances.

Figure 3–Figure supplement 2: **OD weighted mean model**

Correlation between four different models for how single species effects combine into pair effects and the experimental data, with their respective normalized root mean squared error. nRMSE values are calculated from 1000 bootstrapped datasets, and represent the median and interquartile range in parentheses (see Materials and Methods). Similar to Fig. 3B with the addition of the OD weighted mean.

Figure 3–Figure supplement 3: **Distribution of errors for each model predicting pair effects from single species** A) *The accuracy of each model as a function of the difference between the sizes of effect of each individual species within the pair.* B) *Distribution of the prediction accuracy for each model. Dots represent individual measurements, solid lines represent the median, boxes represent the interquartile range, and whiskers are expanded to include values no further than 1.5X interquartile range. The frequencies of these interaction types in the dataset are Negative-Negative 48%, Positive-Positive 14% and Negative-Positive 38%.*

.

Figure 3–Figure supplement 4: **Traits effect on model error**

Pearson correlation value for each trait and the deviation of the model. Correlations with p-values below 0.05 are highlighted with a black frame. See see Materials and Methods for calculations of phenotypic and phylogenetic distances

Figure 3–Figure supplement 5: **Accuracy of all models is reduced when considering only combinations of strains that have weak effects**

Correlation between the different models for how single species effects combine into pair effects, and the experimental data, with their respective normalized root mean squared error. Negative effects and mixed effects were limited to pairs with a combined effect no stronger than -1.2 (the maximum positive effect observed). As the negative-negative and negative-positive predictions become less accurate with these datasets, we posit part of the reason positive-positive interactions were difficult to predict is due to their small effect size.

Figure 3–Figure supplement 6: **Model comparisons stratified by focal species and interaction type**

Correlation between the different models for how single species effects combine, and the experimental data, with their respective normalized root squared mean error. Data is divided for each focal species and interaction type individually.

Figure 4–Figure supplement 1: **OD weighted mean model**

Correlation between four different models for how single species effects combine into trio effects and the experimental data, with their respective normalized root mean squared error. nRMSE values are calculated from 1000 bootstrapped datasets, and represent the median and interquartile range in parentheses (see Materials and Methods). Similar to Fig. 4A with the addition of the OD weighted mean.

References

Altschul, S. F., W. Gish, W. Miller, E. W. Myers, and D. J. Lipman. 1990. “Basic Local Alignment Search Tool.” *Journal of Molecular Biology* 215 (3): 403–10. https://doi.org/10.1016/S0022-2836(05)80360-2.

Arrigo, Kevin R. 2005. “Marine Microorganisms and Global Nutrient Cycles.” *Nature* 437 (7057): 349–55. https://doi.org/10.1038/nature04159.

Barbier, Matthieu, Jean-François Arnoldi, Guy Bunin, and Michel Loreau. 2018. “Generic Assembly Patterns in Complex Ecological Communities.” *Proceedings of the National Academy of Sciences* 115 (9): 2156–61. https://doi.org/10.1073/pnas.1710352115.

Berendsen, Roeland L., Corné M.J. Pieterse, and Peter A.H.M. Bakker. 2012. “The Rhizosphere Microbiome and Plant Health.” *Trends in Plant Science* 17 (8): 478–86. https://doi.org/10.1016/j.tplants.2012.04.001.

Bollenbach, Tobias. 2015. “Antimicrobial Interactions: Mechanisms and Implications for Drug Discovery and Resistance Evolution.” *Current Opinion in Microbiology* 27 (October): 1–9. https://doi.org/10.1016/j.mib.2015.05.008.

Cavicchioli, Ricardo, William J. Ripple, Kenneth N. Timmis, Farooq Azam, Lars R. Bakken, Matthew Baylis, Michael J. Behrenfeld, et al. 2019. “Scientists’ Warning to Humanity: Microorganisms and Climate Change.” *Nature Reviews Microbiology* 17 (9): 569–86. https://doi.org/10.1038/s41579-019-0222-5.

Chang, Chang-Yu, Djordje Bajic, Jean Vila, Sylvie Estrela, and Alvaro Sanchez. 2022. “Emergent Coexistence in Multispecies Microbial Communities.” Preprint. Ecology. https://doi.org/10.1101/2022.05.20.492860.

Cole, James R., Qiong Wang, Jordan A. Fish, Benli Chai, Donna M. McGarrell, Yanni Sun, C. Titus Brown, Andrea Porras-Alfaro, Cheryl R. Kuske, and James M. Tiedje. 2014. “Ribosomal Database Project: Data and Tools for High Throughput RRNA Analysis.” *Nucleic Acids Research* 42 (D1): D633–42. https://doi.org/10.1093/nar/gkt1244.

Cook, K. L., J. L. Garland, A. C. Layton, H. M. Dionisi, L. H. Levine, and G. S. Sayler. 2006. “Effect of Microbial Species Richness on Community Stability and Community Function in a Model Plant-Based Wastewater Processing System.” *Microbial Ecology* 52 (4): 725–37. https://doi.org/10.1007/s00248-006-9105-1.

Elsas, Jan Dirk van, Mario Chiurazzi, Cyrus A. Mallon, Dana Elhottovā, Václav Krištůfek, and Joana Falcão Salles. 2012. “Microbial Diversity Determines the Invasion of Soil by a Bacterial Pathogen.” *Proceedings of the National Academy of Sciences* 109 (4): 1159–64. https://doi.org/10.1073/pnas.1109326109.

Falkowski, P. G., T. Fenchel, and E. F. Delong. 2008. “The Microbial Engines That Drive Earth’s Biogeochemical Cycles.” *Science* 320 (5879): 1034–39. https://doi.org/10.1126/science.1153213.

Fang, Zhen, and Richard L. Smith, eds. 2016. *Production of Biofuels and Chemicals from Lignin*. Biofuels and Biorefineries. Singapore: Springer Singapore. https://doi.org/10.1007/978-981-10-1965-4.

Foster, Kevin R., and Thomas Bell. 2012. “Competition, Not Cooperation, Dominates Interactions among Culturable Microbial Species.” *Current Biology* 22 (19): 1845–50. https://doi.org/10.1016/j.cub.2012.08.005.

Friedman, Jonathan, Logan M. Higgins, and Jeff Gore. 2017. “Community Structure Follows Simple Assembly Rules in Microbial Microcosms.” *Nature Ecology & Evolution* 1 (5): 1–7. https://doi.org/10.1038/s41559-017-0109.

Gilbert, Jack A, Martin J Blaser, J Gregory Caporaso, Janet K Jansson, Susan V Lynch, and Rob Knight. 2018. “Current Understanding of the Human Microbiome.” *Nature Medicine* 24 (4): 392–400. https://doi.org/10.1038/nm.4517.

Gould, Alison L., Vivian Zhang, Lisa Lamberti, Eric W. Jones, Benjamin Obadia, Nikolaos Korasidis, Alex Gavryushkin, Jean M. Carlson, Niko Beerenwinkel, and William B. Ludington. 2018. “Microbiome Interactions Shape Host Fitness.” *Proceedings of the National Academy of Sciences* 115 (51): E11951–60. https://doi.org/10.1073/pnas.1809349115.

Gralka, Matti, Rachel Szabo, Roman Stocker, and Otto X. Cordero. 2020. “Trophic Interactions and the Drivers of Microbial Community Assembly.” *Current Biology* 30 (19): R1176–88. https://doi.org/10.1016/j.cub.2020.08.007.

Guo, Xiaokan, and James Q. Boedicker. 2016. “The Contribution of High-Order Metabolic Interactions to the Global Activity of a Four-Species Microbial Community.” *PLOS Computational Biology* 12 (9): e1005079. https://doi.org/10.1371/journal.pcbi.1005079.

Hsu, Ryan H., Ryan L. Clark, Jin Wen Tan, John C. Ahn, Sonali Gupta, Philip A. Romero, and Ophelia S. Venturelli. 2019. “Microbial Interaction Network Inference in Microfluidic Droplets.” *Cell Systems* 9 (3): 229-242.e4. https://doi.org/10.1016/j.cels.2019.06.008.

Jones, Matt Lloyd, Damian William Rivett, Alberto Pascual-García, and Thomas Bell. 2021. “Relationships between Community Composition, Productivity and Invasion Resistance in Semi-Natural Bacterial Microcosms.” Edited by Bernhard Schmid and Detlef Weigel. *ELife* 10 (October): e71811. https://doi.org/10.7554/eLife.71811.

Kehe, Jared, Anthony Kulesa, Anthony Ortiz, Cheri M. Ackerman, Sri Gowtham Thakku, Daniel Sellers, Seppe Kuehn, Jeff Gore, Jonathan Friedman, and Paul C. Blainey. 2019. “Massively Parallel Screening of Synthetic Microbial Communities.” *Proceedings of the National Academy of Sciences* 116 (26): 12804–9. https://doi.org/10.1073/pnas.1900102116.

Kehe, Jared, Anthony Ortiz, Anthony Kulesa, Jeff Gore, Paul C. Blainey, and Jonathan Friedman. 2021. “Positive Interactions Are Common among Culturable Bacteria.” *Science Advances* 7 (45): eabi7159. https://doi.org/10.1126/sciadv.abi7159.

Köhl, Jürgen, Rogier Kolnaar, and Willem J. Ravensberg. 2019. “Mode of Action of Microbial Biological Control Agents Against Plant Diseases: Relevance Beyond Efficacy.” *Frontiers in Plant Science* 0. https://doi.org/10.3389/fpls.2019.00845.

Konopka, Allan, Stephen Lindemann, and Jim Fredrickson. 2015. “Dynamics in Microbial Communities: Unraveling Mechanisms to Identify Principles.” *The ISME Journal* 9 (7): 1488–95. https://doi.org/10.1038/ismej.2014.251.

Kulesa, Anthony, Jared Kehe, Juan E. Hurtado, Prianca Tawde, and Paul C. Blainey. 2018. “Combinatorial Drug Discovery in Nanoliter Droplets.” *Proceedings of the National Academy of Sciences* 115 (26): 6685–90. https://doi.org/10.1073/pnas.1802233115.

Levine, Jonathan M., Jordi Bascompte, Peter B. Adler, and Stefano Allesina. 2017. “Beyond Pairwise Mechanisms of Species Coexistence in Complex Communities.” *Nature* 546 (7656): 56–64. https://doi.org/10.1038/nature22898.

Mainka, Thomas, David Weirathmüller, Christoph Herwig, and Stefan Pflügl. 2021. “Potential Applications of Halophilic Microorganisms for Biological Treatment of Industrial Process Brines Contaminated with Aromatics.” *Journal of Industrial Microbiology and Biotechnology* 48 (1–2): kuab015. https://doi.org/10.1093/jimb/kuab015.

Manor, Ohad, Chengzhen L. Dai, Sergey A. Kornilov, Brett Smith, Nathan D. Price, Jennifer C. Lovejoy, Sean M. Gibbons, and Andrew T. Magis. 2020. “Health and Disease Markers Correlate with Gut Microbiome Composition across Thousands of People.” *Nature Communications* 11 (1): 5206. https://doi.org/10.1038/s41467-020-18871-1.

Mello Júnior, Carlos Cesar de, Marco Shizuo Owatari, Delano Dias Schleder, Moises Angel Poli, Yan Ramon Rodrigues Gelsleichter, Maiara Postai, Karina Elize Krüger, et al. 2021. “Identification and Characterization of Microorganisms Potentially Beneficial for Intensive Cultivation of Penaeus Vannamei under Biofloc Conditions: Highlighting Exiguobacterium Acetylicum.” *Aquaculture Research* 52 (8): 3628–38. https://doi.org/10.1111/are.15207.

Meroz, Nittay, Nesli Tovi, Yael Sorokin, and Jonathan Friedman. 2021. “Community Composition of Microbial Microcosms Follows Simple Assembly Rules at Evolutionary Timescales.” *Nature Communications* 12 (1): 2891. https://doi.org/10.1038/s41467-021-23247-0.

Mickalide, Harry, and Seppe Kuehn. 2019. “Higher-Order Interaction between Species Inhibits Bacterial Invasion of a Phototroph-Predator Microbial Community.” *Cell Systems* 9 (6):

521-533.e10. https://doi.org/10.1016/j.cels.2019.11.004.
Momeni, Babak, Li Xie, and Wenying Shou. 2017. “Lotka-Volterra Pairwise Modeling Fails to Capture Diverse Pairwise Microbial Interactions.” Edited by Bruce Levin. *ELife* 6 (March): e25051. https://doi.org/10.7554/eLife.25051.
Motarjemi, Yasmine. 2002. “Impact of Small Scale Fermentation Technology on Food Safety in Developing Countries.” *International Journal of Food Microbiology*, Small-Scale Fermentation in Developing Countries, 75 (3): 213–29. https://doi.org/10.1016/S0168-1605(01)00709-7.
Os, Venturelli, Carr Ac, Fisher G, Hsu Rh, Lau R, Bowen Bp, Hromada S, Northen T, and Arkin Ap. 2018. “Deciphering Microbial Interactions in Synthetic Human Gut Microbiome Communities.” *Molecular Systems Biology* 14 (6). https://doi.org/10.15252/msb.20178157.
Palmer, Jacob D., and Kevin R. Foster. 2022. “Bacterial Species Rarely Work Together.” *Science*, May. https://doi.org/10.1126/science.abn5093.
Piccardi, Philippe, Björn Vessman, and Sara Mitri. 2019. “Toxicity Drives Facilitation between 4 Bacterial Species.” *Proceedings of the National Academy of Sciences* 116 (32): 15979–84. https://doi.org/10.1073/pnas.1906172116.
Qi, Shan Shan, Alexander Bogdanov, Margo Cnockaert, Tessa Acar, Sarah Ranty-Roby, Tom Coenye, Peter Vandamme, Gabriele M. König, Max Crüsemann, and Aurélien Carlier. 2021. “Induction of Antibiotic Specialized Metabolism by Co-Culturing in a Collection of Phyllosphere Bacteria.” *Environmental Microbiology* 23 (4): 2132–51. https://doi.org/10.1111/1462-2920.15382.
Qian, Jimmy J., and Erol Akçay. 2020. “The Balance of Interaction Types Determines the Assembly and Stability of Ecological Communities.” *Nature Ecology & Evolution* 4 (3): 356–65. https://doi.org/10.1038/s41559-020-1121-x.
Ro, Dae-Kyun, Eric M. Paradise, Mario Ouellet, Karl J. Fisher, Karyn L. Newman, John M. Ndungu, Kimberly A. Ho, et al. 2006. “Production of the Antimalarial Drug Precursor Artemisinic Acid in Engineered Yeast.” *Nature* 440 (7086): 940–43. https://doi.org/10.1038/nature04640.
Sanchez, Alvaro. 2019. “Defining Higher-Order Interactions in Synthetic Ecology: Lessons from Physics and Quantitative Genetics.” *Cell Systems* 9 (6): 519–20. https://doi.org/10.1016/j.cels.2019.11.009.
Sanchez-Gorostiaga, Alicia, Djordje Bajić, Melisa L. Osborne, Juan F. Poyatos, and Alvaro Sanchez. 2019. “High-Order Interactions Distort the Functional Landscape of Microbial Consortia.” Edited by Wenying Shou. *PLOS Biology* 17 (12): e3000550. https://doi.org/10.1371/journal.pbio.3000550.
Tyc, Olaf, Marlies van den Berg, Saskia Gerards, Johannes A. van Veen, Jos M. Raaijmakers, Wietse de Boer, and Paolina Garbeva. 2014. “Impact of Interspecific Interactions on Antimicrobial Activity among Soil Bacteria.” *Frontiers in Microbiology* 5 (October). https://doi.org/10.3389/fmicb.2014.00567.
Varjani, Sunita J., Edgard Gnansounou, and Ashok Pandey. 2017. “Comprehensive Review on Toxicity of Persistent Organic Pollutants from Petroleum Refinery Waste and Their Degradation by Microorganisms.” *Chemosphere* 188 (December): 280–91. https://doi.org/10.1016/j.chemosphere.2017.09.005.
Vetsigian, Kalin, Rishi Jajoo, and Roy Kishony. 2011. “Structure and Evolution of Streptomyces Interaction Networks in Soil and In Silico.” *PLOS Biology* 9 (10): e1001184. https://doi.org/10.1371/journal.pbio.1001184.
Westhoff, Sanne, Alexander M. Kloosterman, Stephan F. A. van Hoesel, Gilles P. van Wezel, and Daniel E. Rozen. 2021. “Competition Sensing Changes Antibiotic Production in Streptomyces.” *MBio* 12 (1): e02729-20. https://doi.org/10.1128/mBio.02729-20.

Widder, Stefanie, Rosalind J. Allen, Thomas Pfeiffer, Thomas P. Curtis, Carsten Wiuf, William T. Sloan, Otto X. Cordero, et al. 2016. “Challenges in Microbial Ecology: Building Predictive Understanding of Community Function and Dynamics.” *The ISME Journal* 10 (11): 2557–68. https://doi.org/10.1038/ismej.2016.45.

Wootton, J.Timothy. 2002. “Indirect Effects in Complex Ecosystems: Recent Progress and Future Challenges.” *Journal of Sea Research* 48 (2): 157–72. https://doi.org/10.1016/S1385-1101(02)00149-1.

Fluorescence assays

To test the accuracy of using fluorescence to assay interactions, we performed the following experiment correlating effect size as measured by fluorescent signal to effect size as measured by OD_{600}. Bacterial strains were seeded from -80 stock directly into 0.5 ml LB medium in a 96 well plate, and grown overnight at 30°C at 900 RPM (on a Titramax 100). Cells were washed 3 times by centrifugation at 3600 rcf for three minutes, removal of supernatant, and resuspension in M9 minimal media (with the addition of 1% [w/v] glucose). All cultures were normalized to 0.02 OD_{600}. HTD96b plates (HTDialysis, Gales Ferry, CT, USA) with membranes containing 1 µm pores splitting each well were seeded with 150 µl affecting species and focal species cultures on opposite sides of the membrane. After a 24 hour growth period at 30°C, shaking at 600 RPM, 100 µl of culture for each side of each well was transferred to a standard 96-well plate and OD_{600} and fluorescence were measured (Appendix 1, Figure 1). Each interaction was measured using three technical replicates.

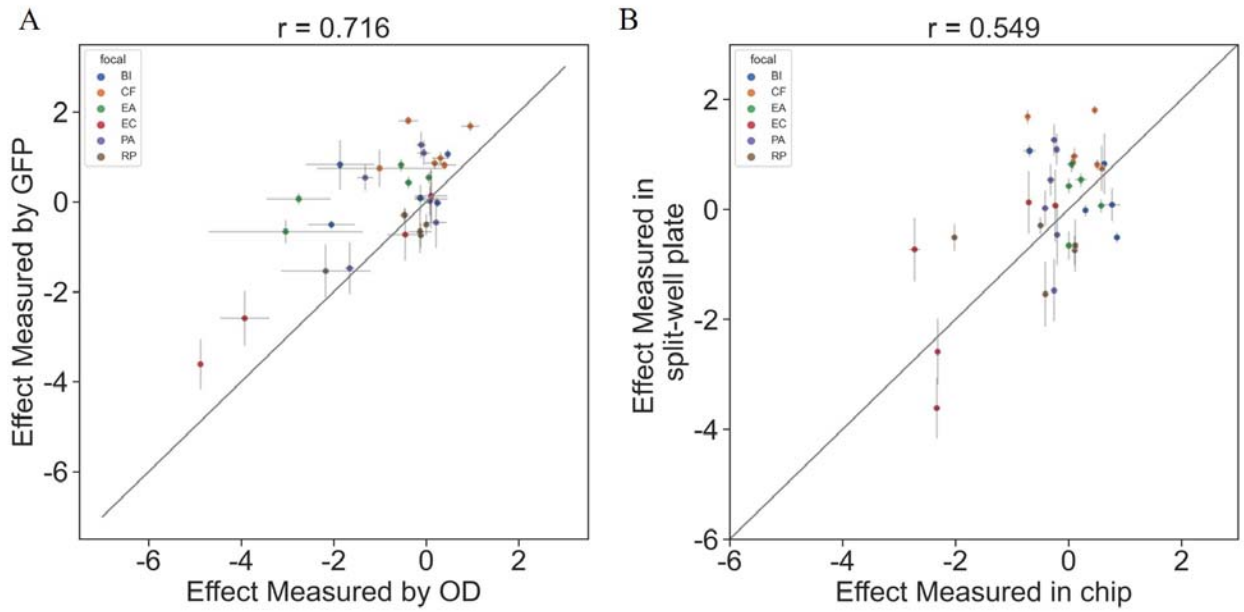

Appendix 1, Figure 1: **Interactions measured with OD_{600} are consistent with those based on fluorescent measurements**

The effects of six single species on each focal were measured using OD_{600} and fluorescence in a 96 split well plate (see Materials and Methods). A) The correlation between the effect when measured by fluorescence and OD600 (p=1e-6). B) The correlation between the effect when measured in the kChip and the HTD Equilibrium Dialysis System (p=0.001).

To ensure that model accuracy was not influenced by (fluorescent) measurement limitations, we analyzed the competitive effects of models with predictions limited to the range of minimal observed measurements (as we know the maximal measurements were not near saturation). This affected only the additive model (which was the only model that could predict effects stronger than those observed), and its accuracy was improved, but it was still less accurate than the mean and strongest models (Appendix 1, Figure 2).

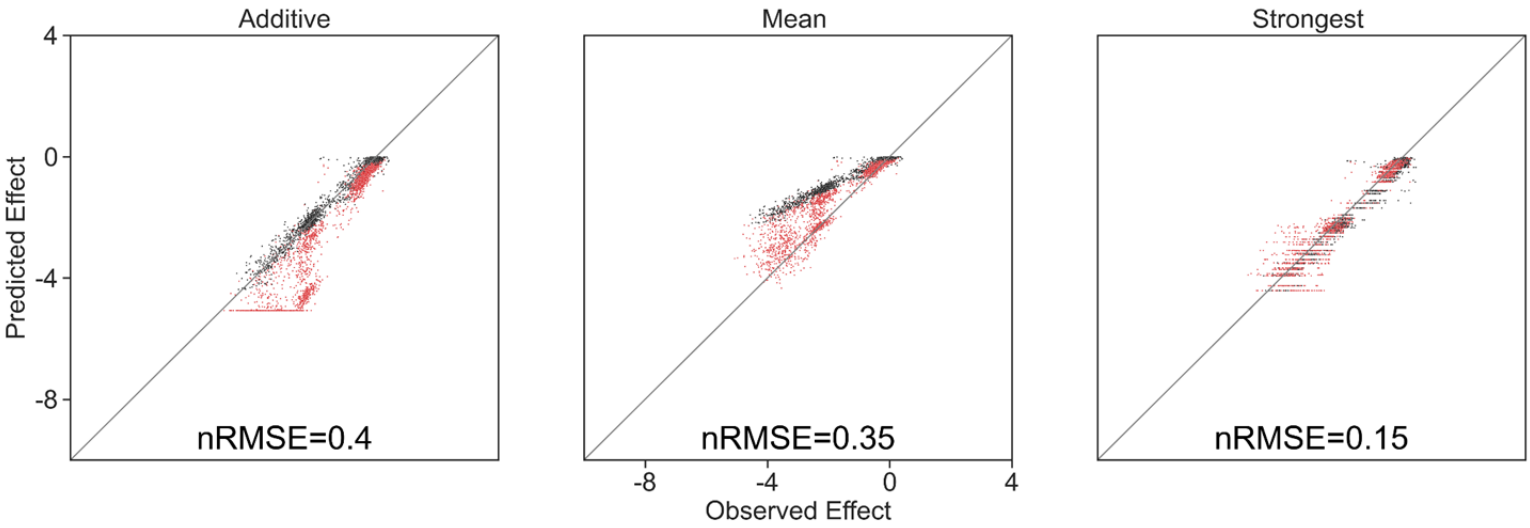

Appendix 1, Figure 2: **Model predictions limited by the lowest observed effect**
Correlation between three different models for how single species effects combine, and the experimental data, with their respective normalized root squared mean error. Model predictions were limited to the minimal observed effects, and only data for negative predictions are shown.

Additionally, an experiment was carried out in the kChip to measure autofluorescence of affecting species. This setup was identical to the droplet preparation and culturing protocol detailed above, except that cultures were not mixed with the focal species prior to droplet generation. In this setup each droplet contains a single species, and wells contain one or two species (depending on whether the droplets were from the same or different cultures). Isolates were only used with focals whose monocultures were at least five times larger than the isolates autofluorescence signal, allowing to measure effects of at least -1.5. Full datasets without autofluorescence filtering can be seen in Appendix 1, Figure 3.

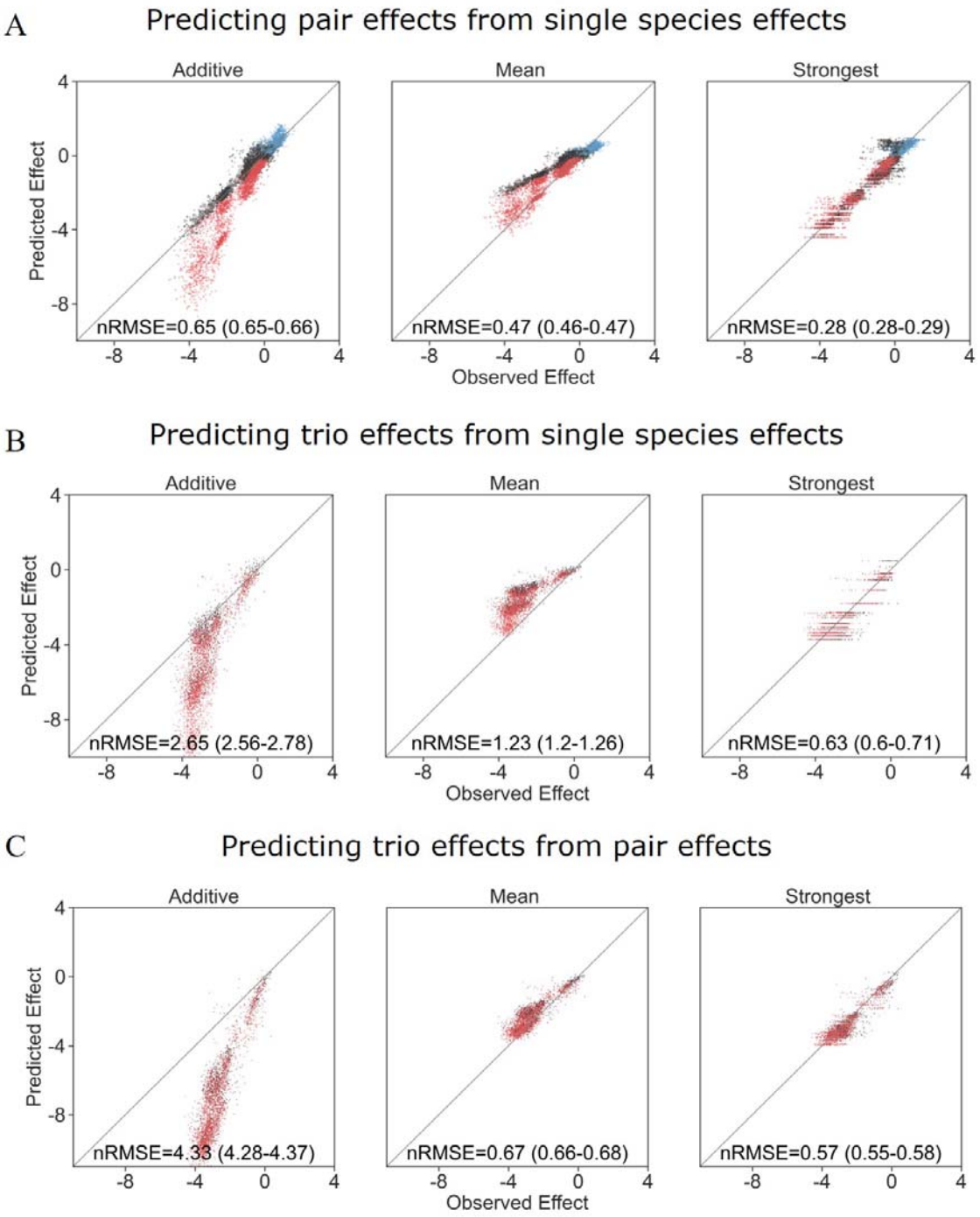

Appendix 1, Figure 3: **Different models prediction accuracy using all measured effects, not filtered for affecting species autofluorescence**

Correlation between three different models for how A) single species effects combine to pairs B) single species effects combine into trio effects and C) pairwise species effects combine into trio effects, and the experimental data. Root squared mean error normalized to the interquartile range. nRMSE values are calculated from 1000 datasets, and represent the median and interquartile range in parentheses (see Materials and Methods).

A

Library of 61 strains, of which 6 focal species were fluorescently labeled

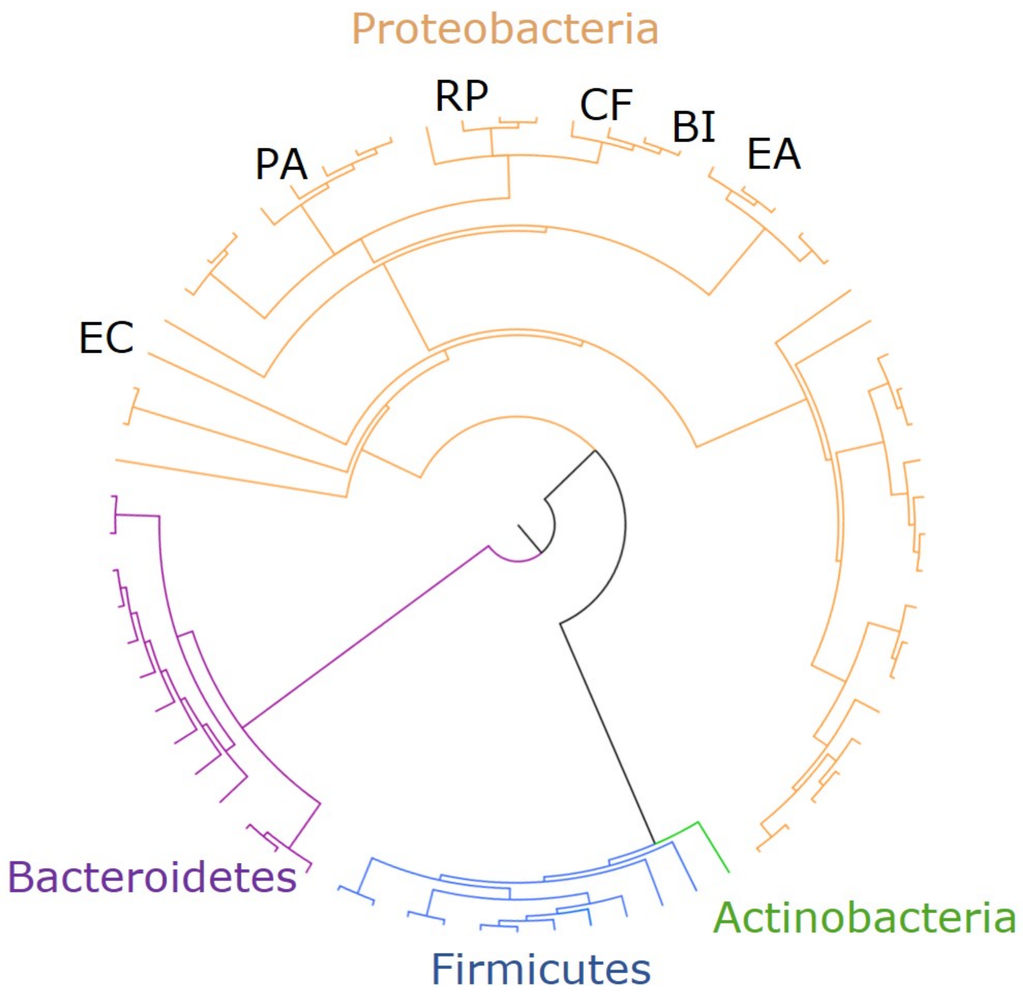

B

One way effects on focal species were measured

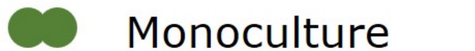

Effects of Singles Species

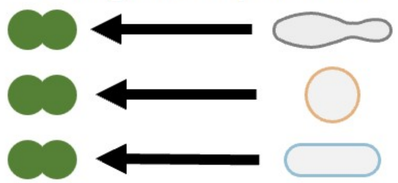

6 focals x ~60 species

Effects of Pairs

6 focals x ~1700 pairs

Effects of Trios

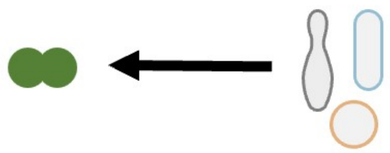

1 focal x 3755 trios

C

Single species data were used to predict combined effects

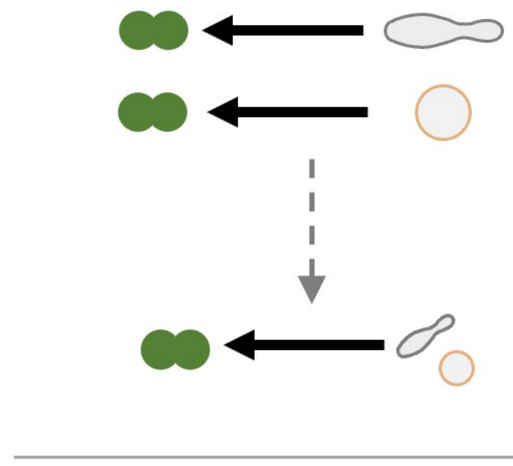

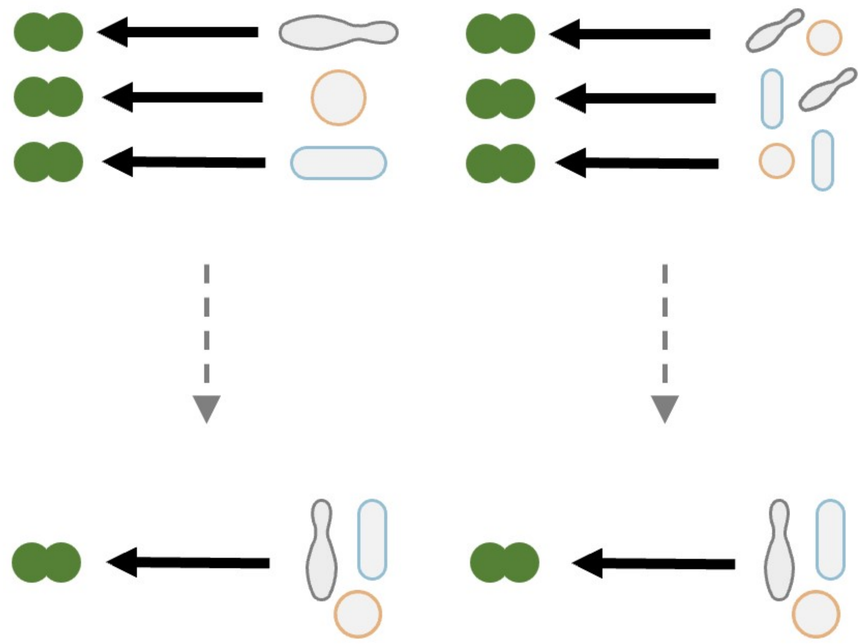

D

$$\text{Effect} = \log\left(\frac{\text{Focal coculture growth}}{\text{Focal monoculture growth}}\right)$$

Types of Droplets

Focal monoculture

Focal + affecting species

Blank

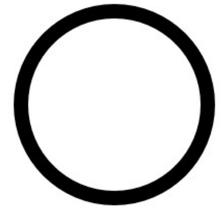

Focal monoculture
Two droplets per well

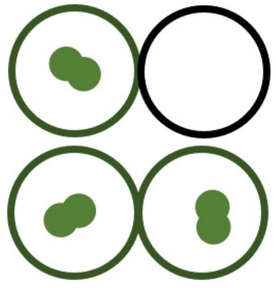

Focal monoculture
Three droplets per well

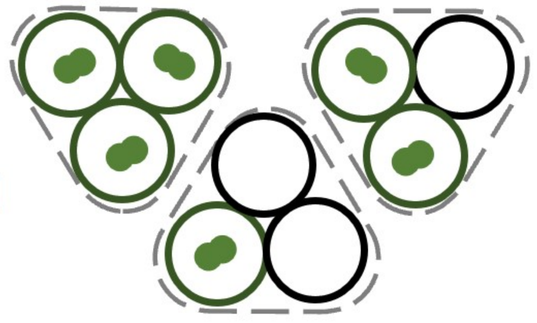

Single species effects
Two droplets per well

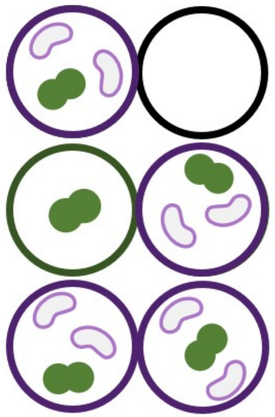

Focal:Affecting1

1:2

1:1

1:2

Single species effects
Three droplets per well

Focal:Affecting1

1:2 1:1

3:4 3:2

Pair effects
Two droplets per well

Focal:Affecting1:Affecting2

1:1:1

Pair effects
Three droplets per well

Focal:Affecting1:Affecting2

3:4:2 1:1:1

3:2:2

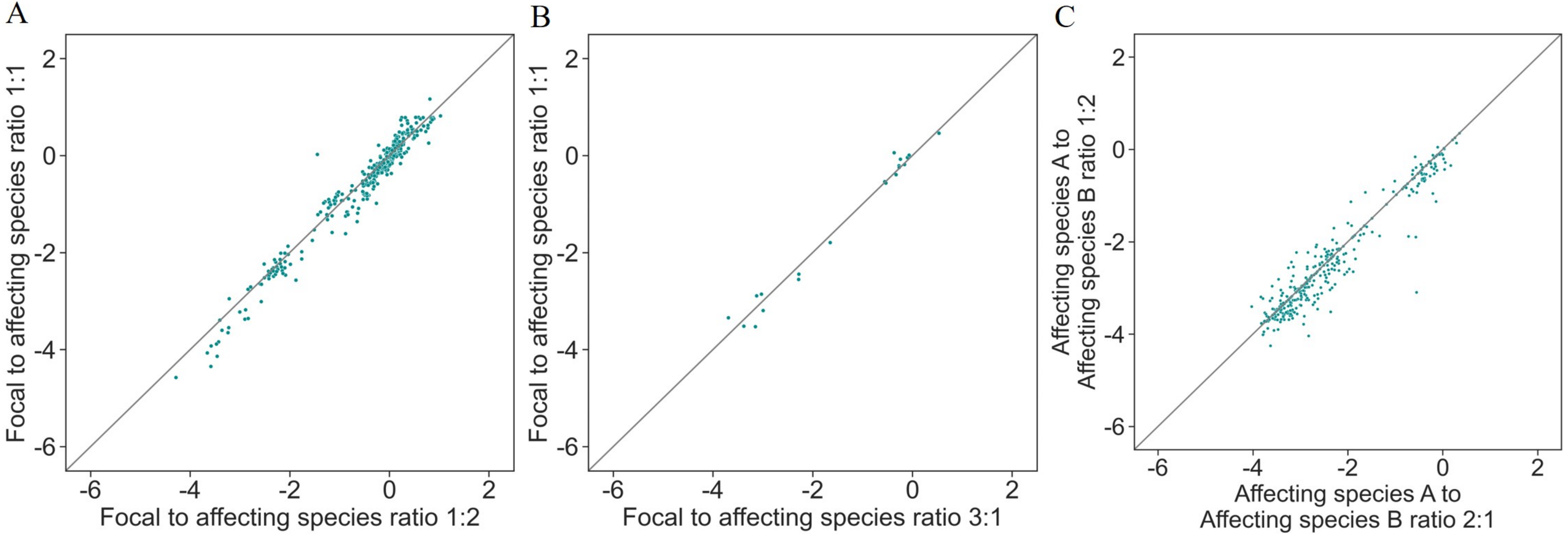
A
Focal to affecting species ratio 1:1
Focal to affecting species ratio 1:2
2
0
-2
-4
-6
-6
-4
-2
0
2
B
Focal to affecting species ratio 1:1
Focal to affecting species ratio 3:1
C
Affecting species A to Affecting species B ratio 1:2
Affecting species A to Affecting species B ratio 2:1

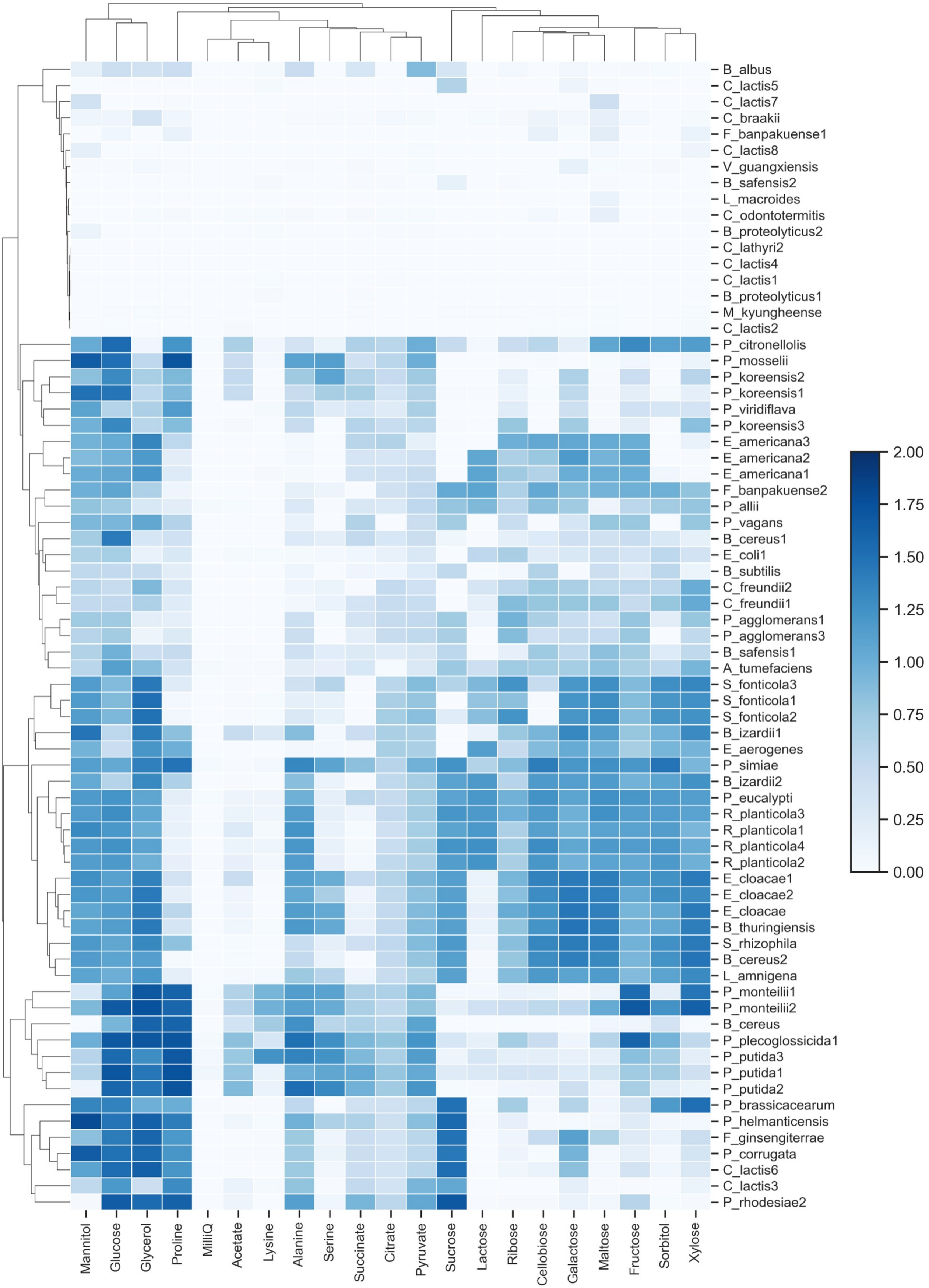
B_albus
C_lactis5
C_lactis7
C_braakii
F_banpakuense1
C_lactis8
V_guangxiensis
B_safensis2
L_macroides
C_odontotermitis
B_proteolyticus2
C_lathyri2
C_lactis4
C_lactis1
B_proteolyticus1
M_kyungheense
C_lactis2
P_citronellolis
P_mosselii
P_koreensis2
P_koreensis1
P_viridiflava
P_koreensis3
E_americana3
E_americana2
E_americana1
F_banpakuense2
P_allii
P_vagans
B_cereus1
E_coli1
B_subtilis
C_freundii2
C_freundii1
P_agglomerans1
P_agglomerans3
B_safensis1
A_tumefaciens
S_fonticola3
S_fonticola1
S_fonticola2
B_izardii1
E_aerogenes
P_simiae
B_izardii2
P_eucalypti
R_planticola3
R_planticola1
R_planticola4
R_planticola2
E_cloacae1
E_cloacae2
E_cloacae
B_thuringiensis
S_rhizophila
B_cereus2
L_amnigena
P_monteilii1
P_monteilii2
B_cereus
P_plecoglossicida1
P_putida3
P_putida1
P_putida2
P_brassicacearum
P_helmanticensis
F_ginsengiterrae
P_corrugata
C_lactis6
C_lactis3
P_rhodesiae2
2.00
1.75
1.50
1.25
1.00
0.75
0.50
0.25
0.00
Mannitol
Glucose
Glycerol
Proline
MilliQ
Acetate
Lysine
Alanine
Serine
Succinate
Citrate
Pyruvate
Sucrose
Lactose
Ribose
Cellobiose
Galactose
Maltose
Fructose
Sorbitol
Xylose

P_rhodesiae2
P_helmanticensis
P_simiae
P_monteilii1
B_cereus1
P_putida2
P_mosselii
P_koreensis1
P_putida3
P_monteilii2
P_putida1
P_plecoglossicida
P_koreensis2
P_koreensis3
C_lactis6
F_ginsengiterrae
B_cereus
P_corrugata
P_brassicacearum
P_eucalypti
R_planticola3
P_citronellolis
C_freundii1
C_lactis3
R_planticola4
R_planticola2
R_planticola1
E_americana1
B_izardii1
E_cloacae1
B_cereus2
E_cloacae
E_cloacae2
B_thuringiensis
S_rhizophila
L_amnigena
S_fonticola1
E_americana3
S_fonticola2
S_fonticola3
E_americana2
P_vagans
A_tumefaciens
P_allii
B_albus
C_freundii2
P_agglomerans1
P_agglomerans3
C_lactis2
E_coli1
C_braakii
B_proteolyticus2
C_lactis7
C_lactis5
V_guangxiensis
C_lactis1
M_kyungheense
L_macroides
B_subtilis
C_odontotermitis
B_safensis2
C_lathyri2
B_proteolyticus1
C_lactis4
C_lactis8
F_banpakuense1
E_aerogenes
P_viridiflava
B_safensis1
F_banpakuense2
B_izardii2

2.00
1.75
1.50
1.25
1.00
0.75
0.50
0.25
0.00

Gentamicin
Kanamycin
Rifampicin
Streptomycin
Vancomycin
Ampicillin
Carbenicillin
Chloramphenicol
Trimethoprim
Amoxicillin
Spectinomycin

EC

EA

RP

BI

CF

PA

Fluorescent signal [A.U.]

10^0

10^1

10^2

10^3

0

24

48

72

Time [hours]

A

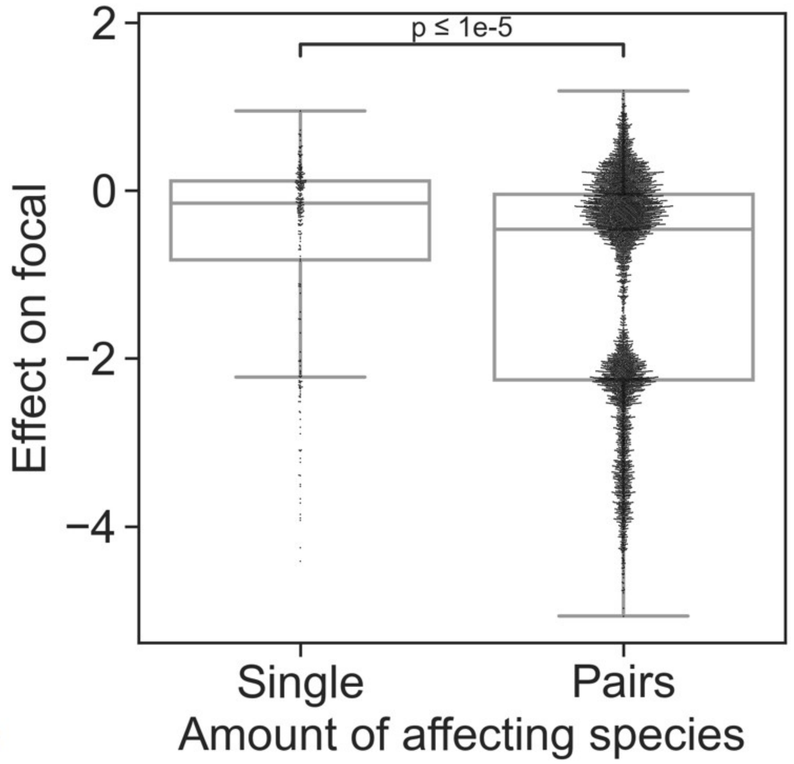
p ≤ 1e-5
Effect on focal
2
0
−2
−4
Single
Pairs
Amount of affecting species

B

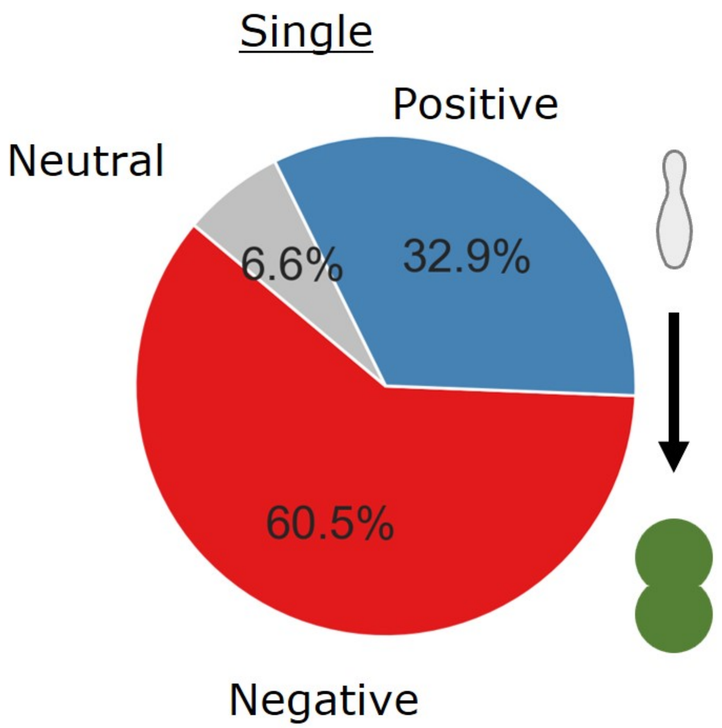
Single
Positive
Neutral
6.6%
32.9%
60.5%
Negative

C

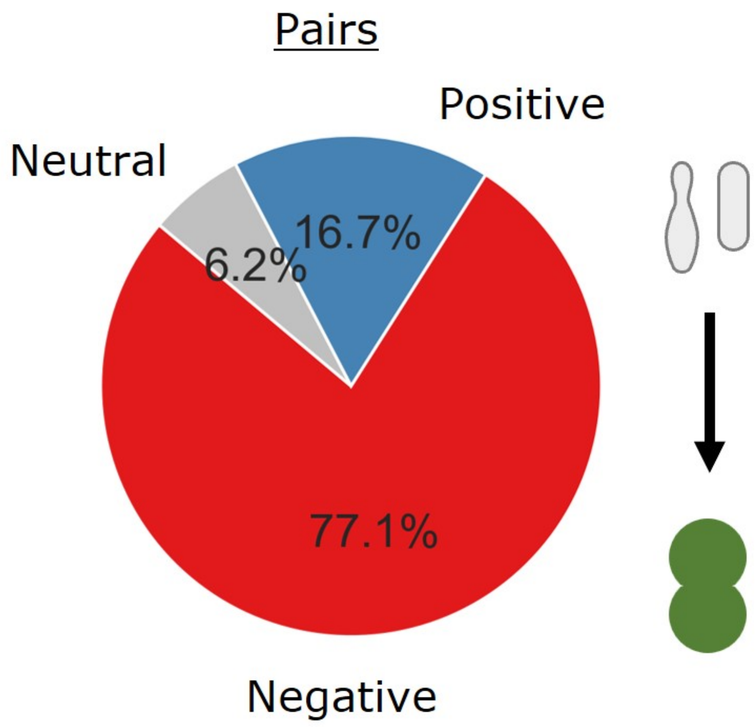
Pairs
Positive
Neutral
6.2%
16.7%
77.1%
Negative

D

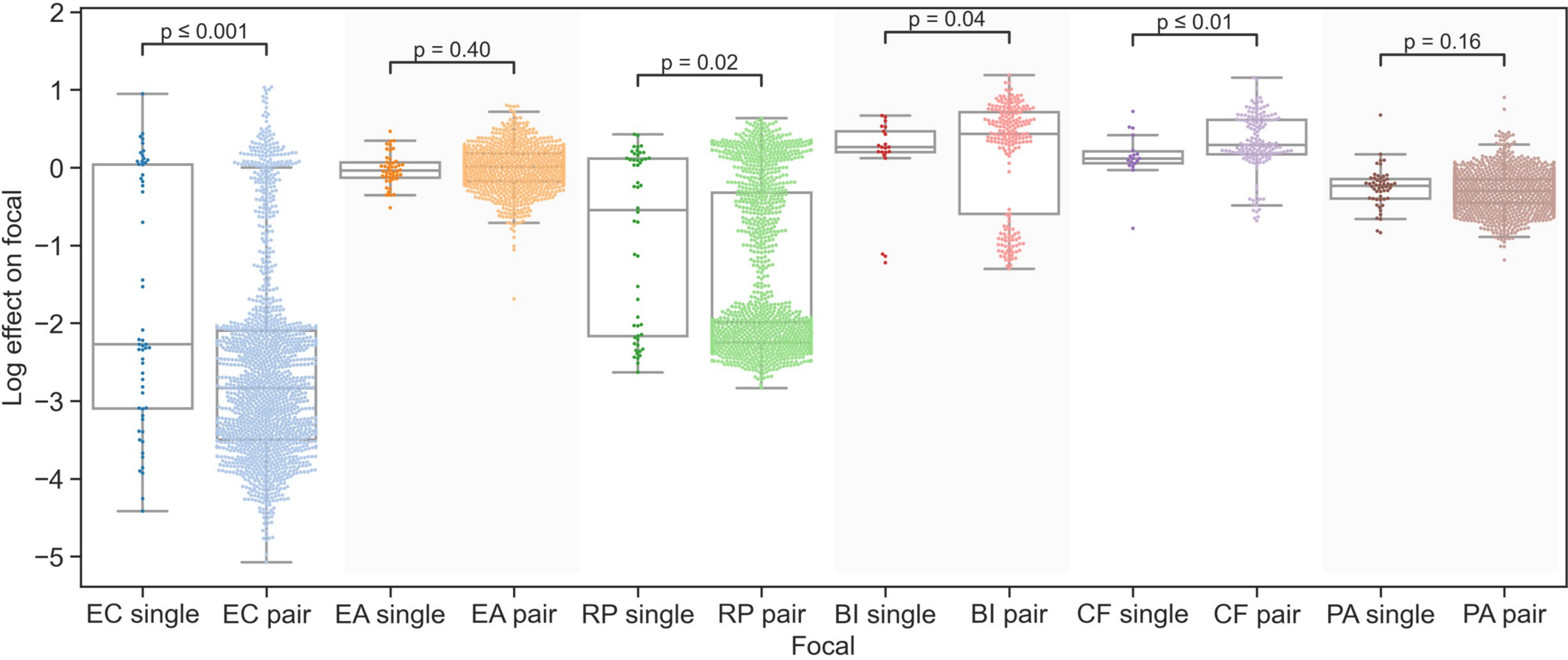
p ≤ 0.001
p = 0.40
p = 0.02
p = 0.04
p ≤ 0.01
p = 0.16
Log effect on focal
2
1
0
−1
−2
−3
−4
−5
EC single
EC pair
EA single
EA pair
RP single
RP pair
BI single
BI pair
CF single
CF pair
PA single
PA pair
Focal

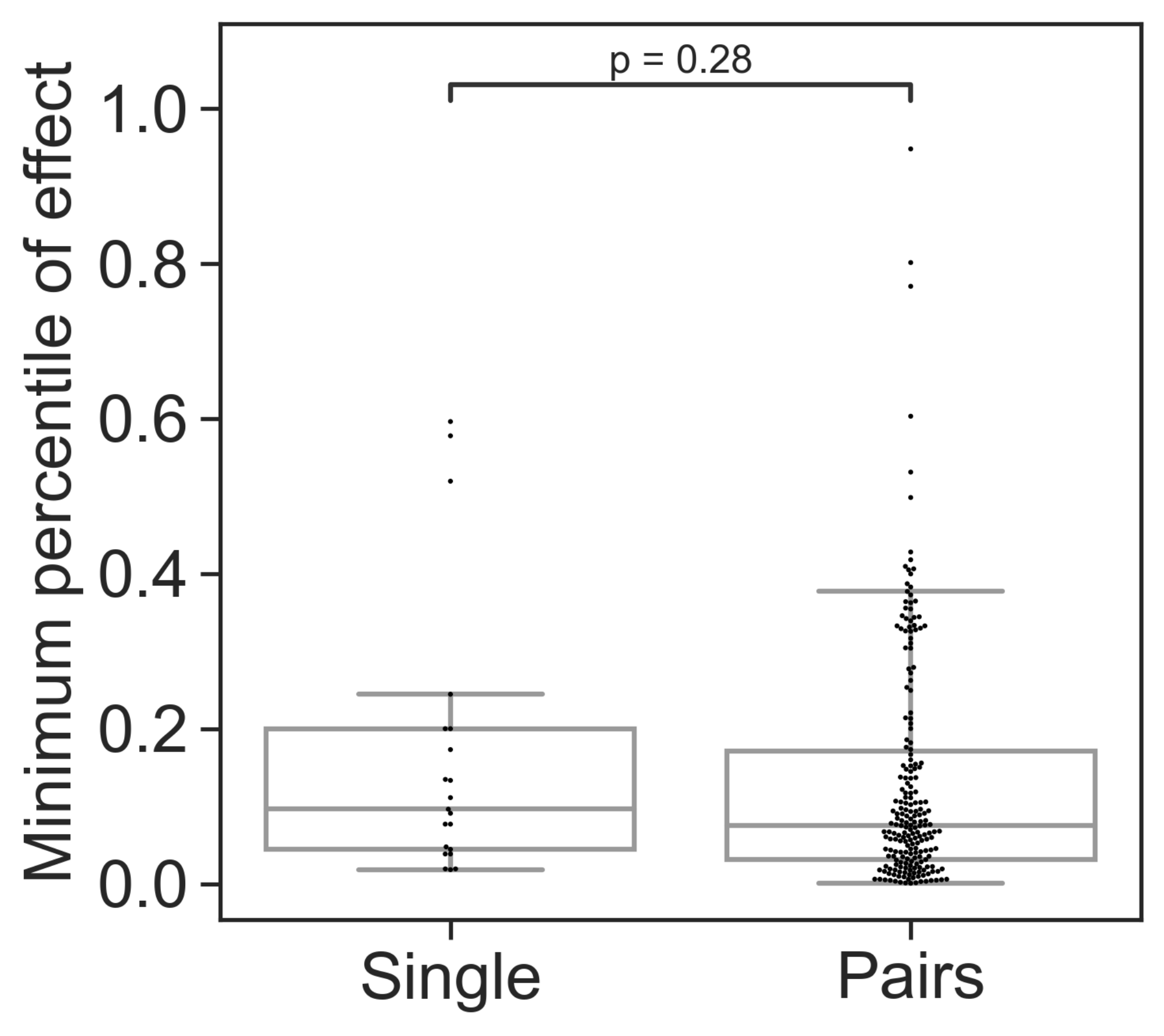
p = 0.28
Minimum percentile of effect
1.0
0.8
0.6
0.4
0.2
0.0
Single
Pairs

A

$$Effect_{ab} = Effect_a + Effect_b \qquad Effect_{ab} = \frac{Effect_a + Effect_b}{2} \qquad Effect_{ab} = \underset{E \in [Effect_a, Effect_b]}{argmax} |E|$$

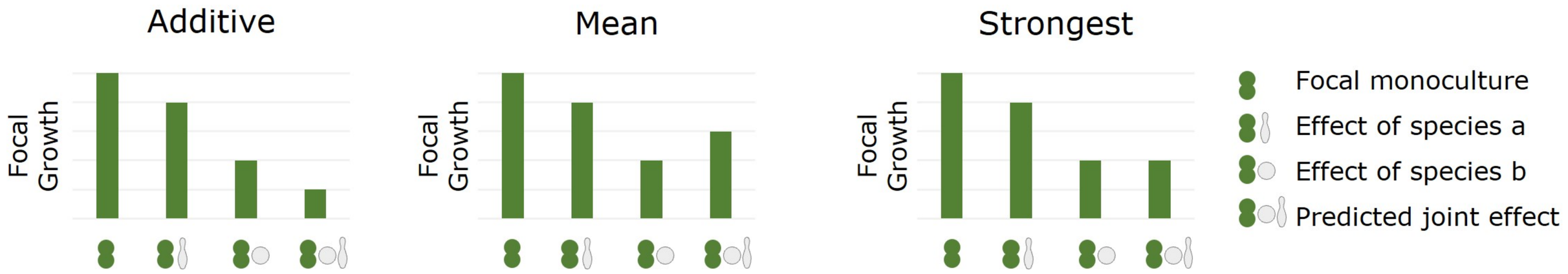

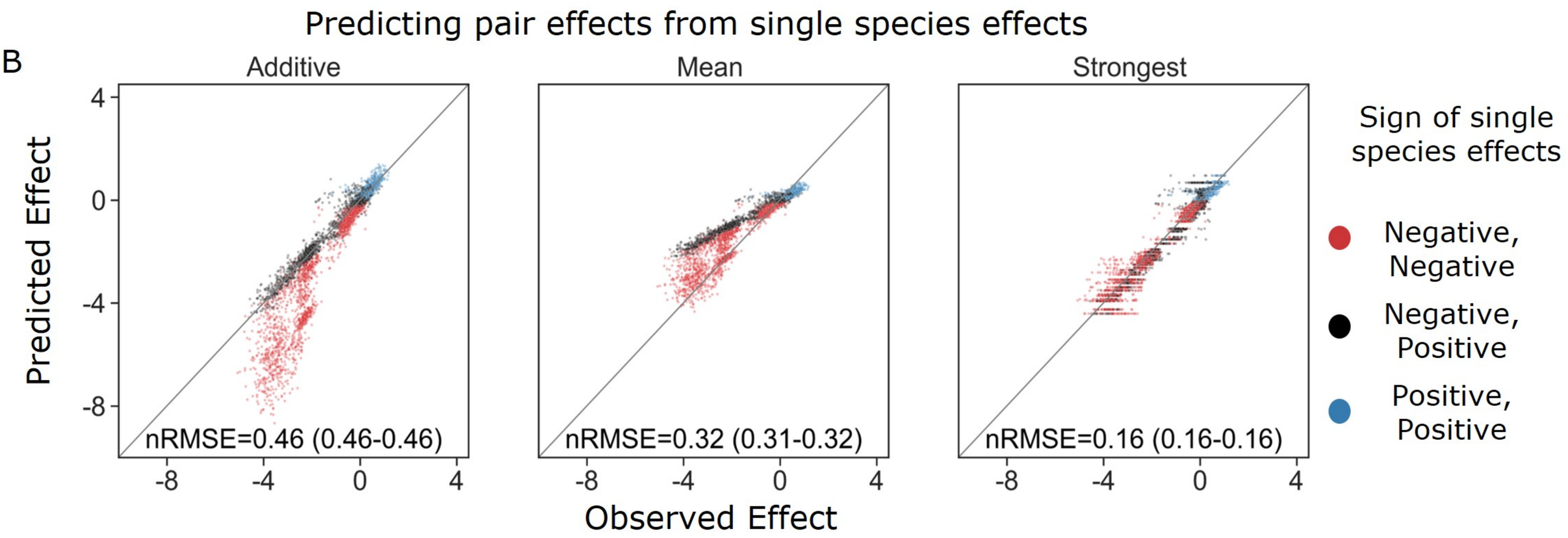

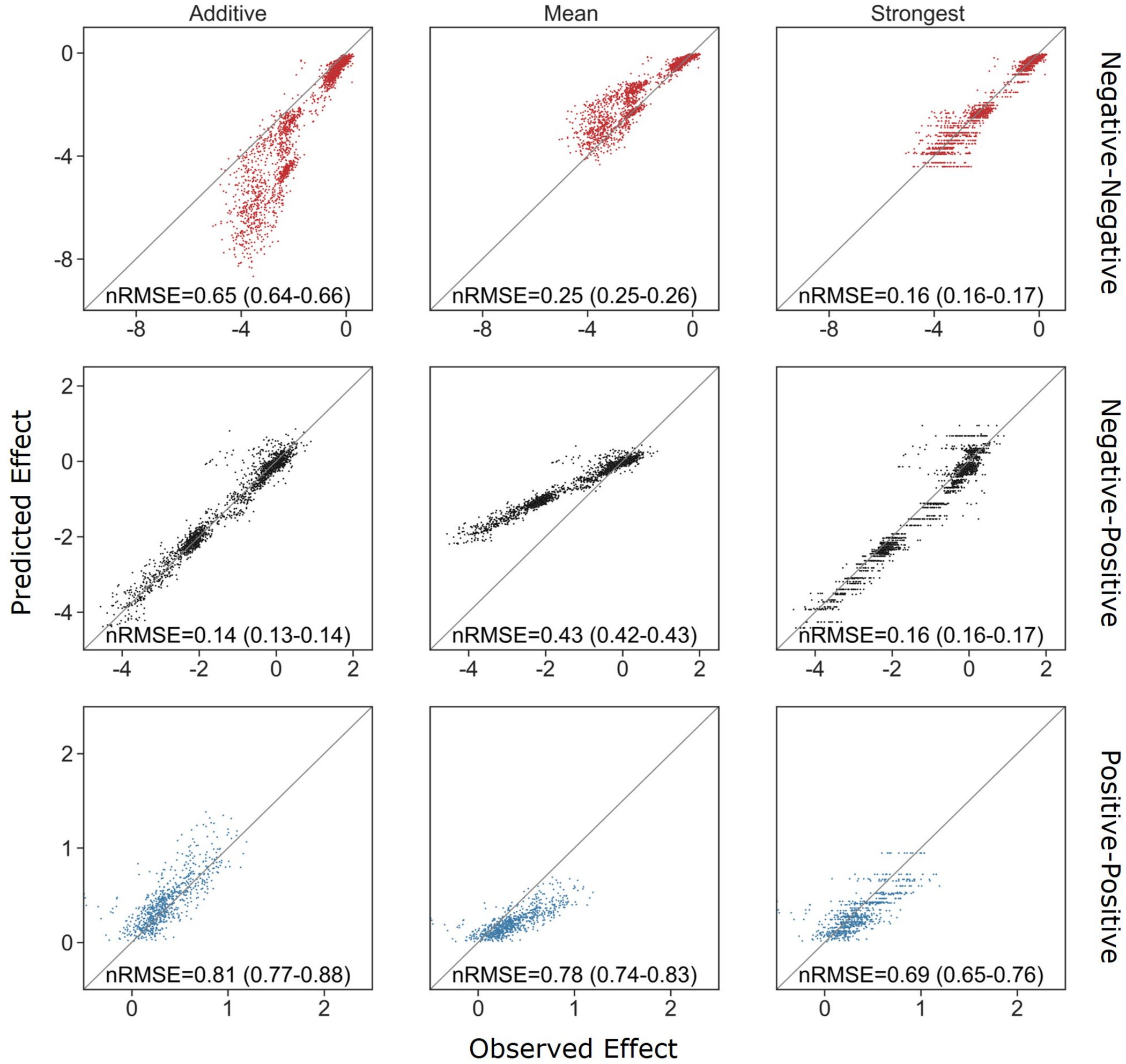

A

	EC	EA	RP	BI	CF	PA
Metabolic distance from focal	0.369	0.257	0.403	0.026	-0.230	0.168
Resistance distance from focal	-0.146	-0.059	0.269	-0.006	-0.283	-0.078
Phylogenetic distance from focal	0.760	0.384	0.667	0.069	-0.293	0.204
Maximum OD	-0.557	-0.253	-0.631	-0.255	0.143	-0.246
Affecting species growth rate	-0.625	-0.459	-0.446	-0.192	0.298	-0.432

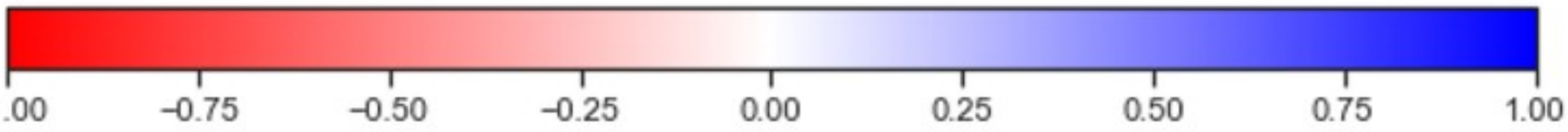

B

	EC	EA	RP	BI	CF	PA
Affecting species metabolic distance	-0.051	0.002	0.047	-0.056	0.126	-0.032
Affecting species resistance distance	-0.145	-0.208	-0.026	-0.469	-0.048	-0.005
Affecting species phylogentic distance	0.086	0.132	0.117	-0.060	0.016	0.078
Mean metabolic distance from focal	0.288	0.323	0.150	0.316	0.203	0.044
Mean resistance distance from focal	-0.126	-0.117	0.209	0.018	-0.059	-0.147
Mean phylogentic distance from focal	0.669	0.489	0.476	0.424	0.042	0.184

Additive

Mean

OD Weighted

Strongest

Predicted Effect

Observed Effect

4

0

-4

-8

nRMSE=0.46 (0.46-0.46)

nRMSE=0.32 (0.31-0.32)

nRMSE=0.24 (0.23-0.24)

nRMSE=0.16 (0.16-0.16)

Sign of single species effects

Negative, Negative

Negative, Positive

Positive, Positive

A

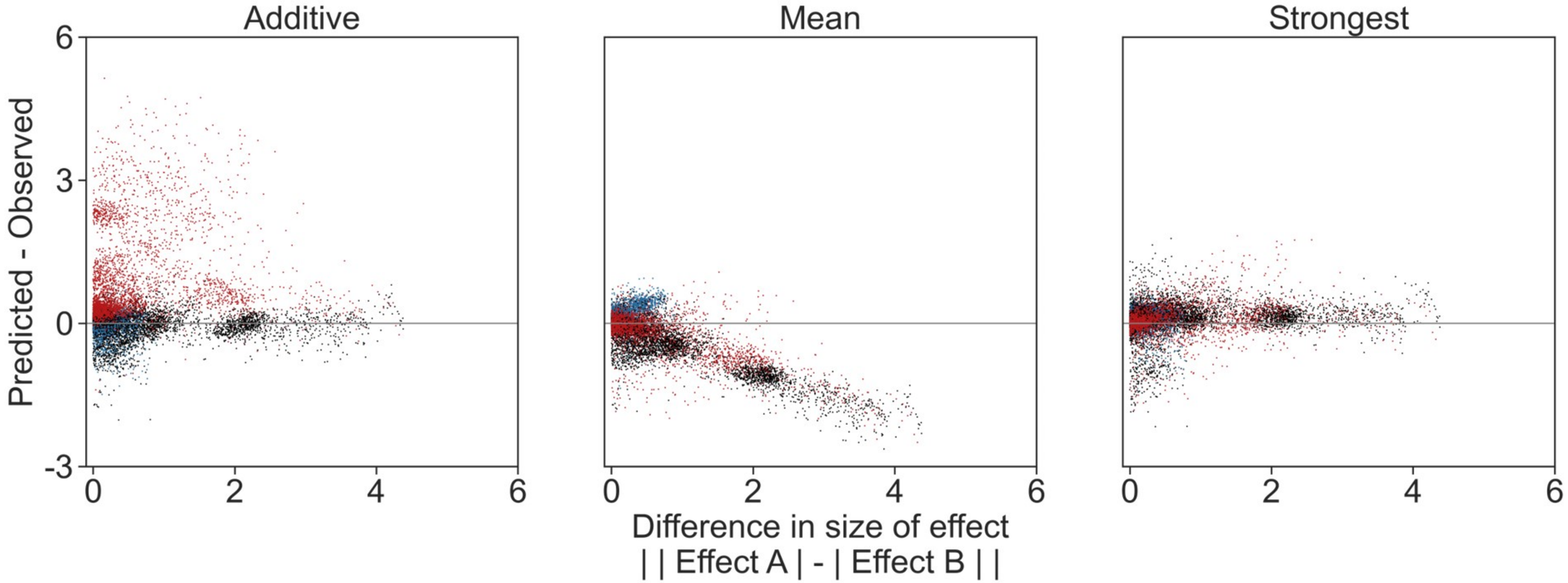

Qualitative single species effects

- Negative, Negative
- Negative, Positive
- Positive, Positive

B

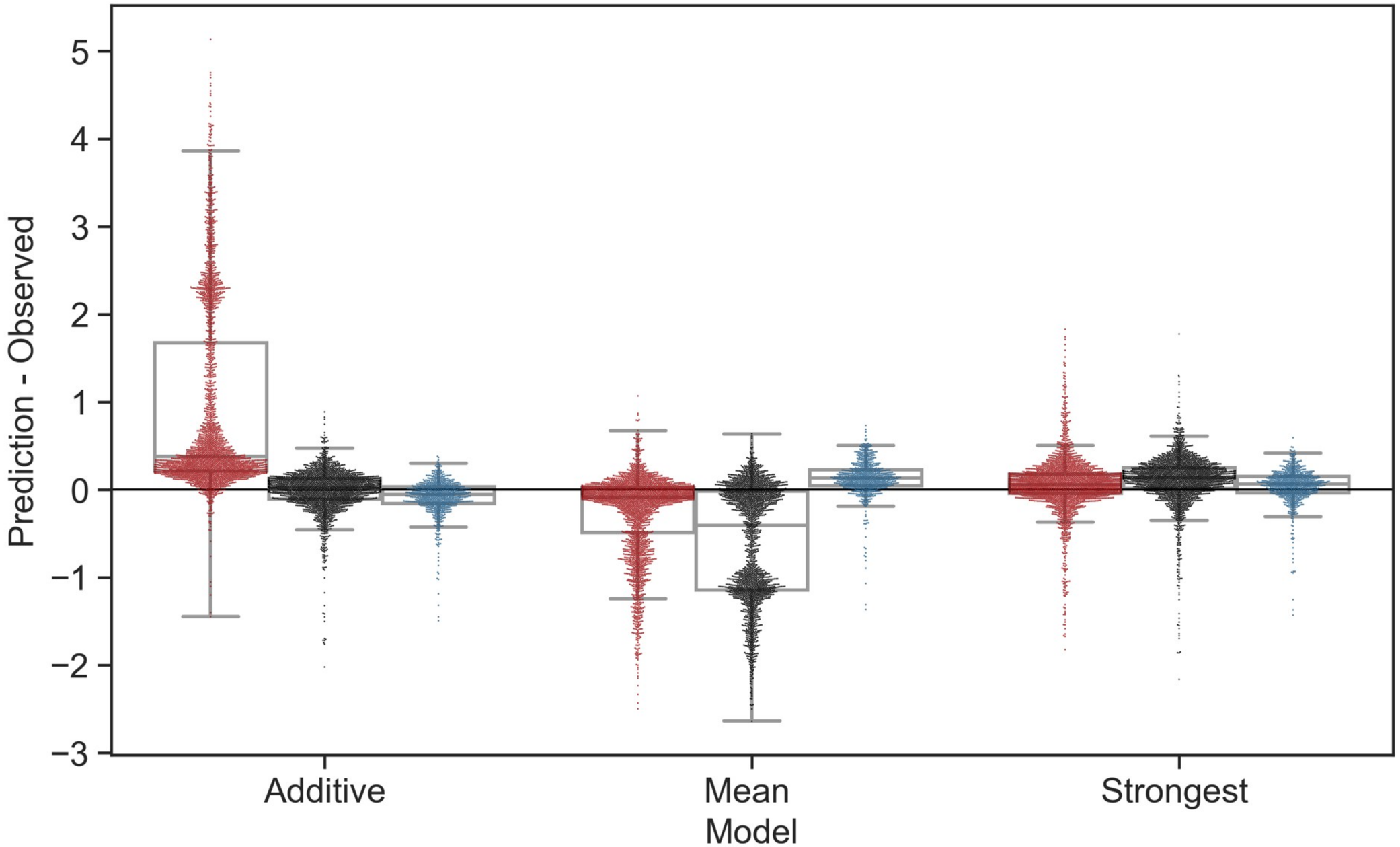

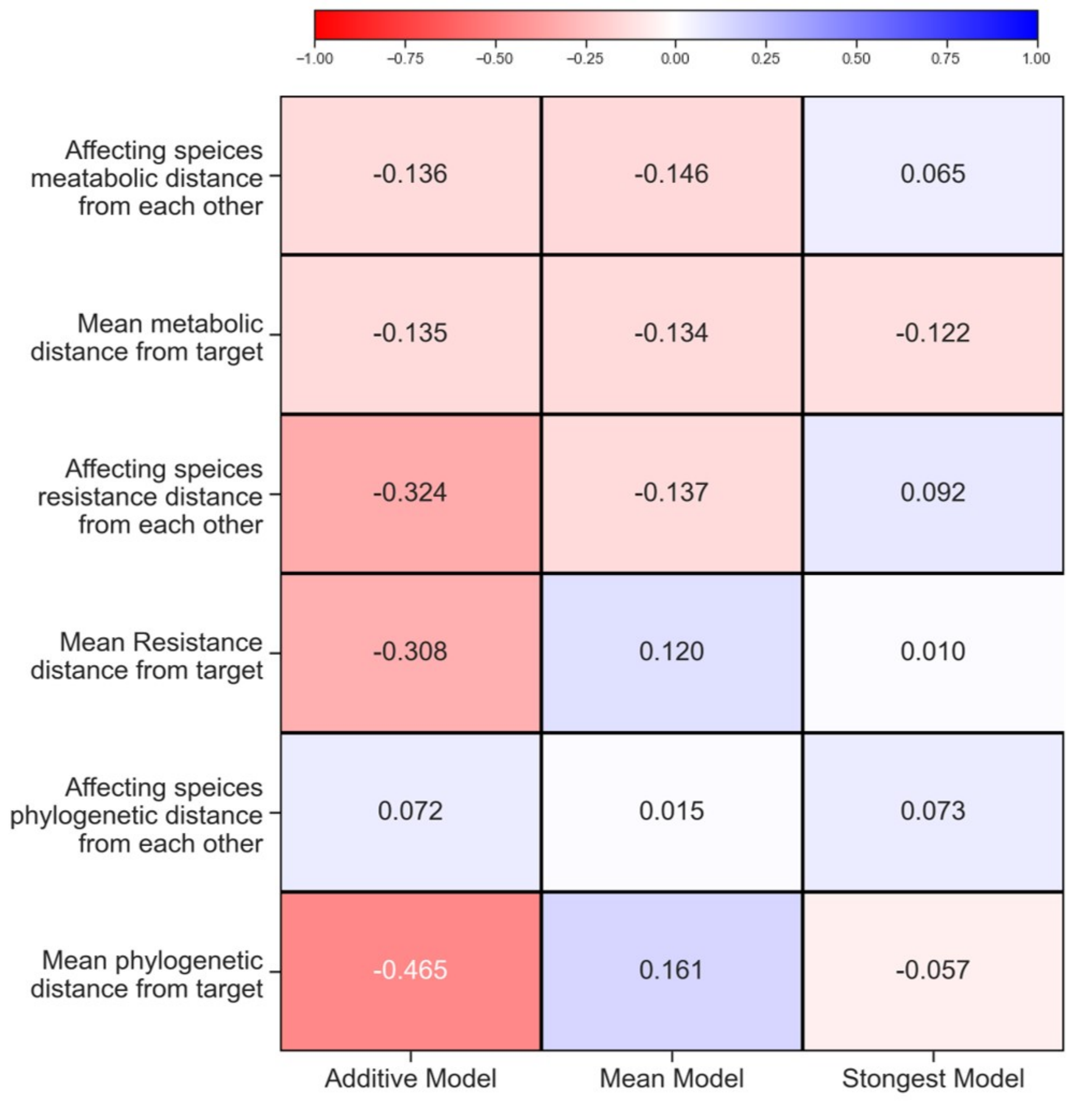
−1.00
−0.75
−0.50
−0.25
0.00
0.25
0.50
0.75
1.00
Affecting speices meatabolic distance from each other
-0.136
-0.146
0.065
Mean metabolic distance from target
-0.135
-0.134
-0.122
Affecting speices resistance distance from each other
-0.324
-0.137
0.092
Mean Resistance distance from target
-0.308
0.120
0.010
Affecting speices phylogenetic distance from each other
0.072
0.015
0.073
Mean phylogenetic distance from target
-0.465
0.161
-0.057
Additive Model
Mean Model
Stongest Model

Additive

Mean

Strongest

Negative-Negative

nRMSE=1.06

nRMSE=0.45

nRMSE=0.52

Predicted Effect

Negative-Positive

nRMSE=0.53

nRMSE=0.57

nRMSE=0.77

Positive-Positive

nRMSE=0.66

nRMSE=0.74

nRMSE=0.61

Observed Effect

EC
EA
RP
BI
CF
PA
Additive
Mean
Strongest
2.0
0.75
4.04
14.38
0.13
1.11
0.78
0.6
1.37
0.99
0.28
0.44
0.47
0.58
0.58
0.86
0.1
0.49
Negative-Negative
Predicted Effect
0.27
0.62
0.1
1.03
0.34
0.83
1.05
0.67
0.54
2.35
0.33
0.66
0.32
0.76
0.14
1.68
0.55
1.29
Negative-Positive
1.2
0.91
0.73
0.51
0.36
1.82
0.93
0.89
0.93
0.78
0.64
1.06
0.99
0.88
0.68
0.54
0.39
1.64
Positive-Positive
Observed Effect

Predicting trio effects from single species effects

A

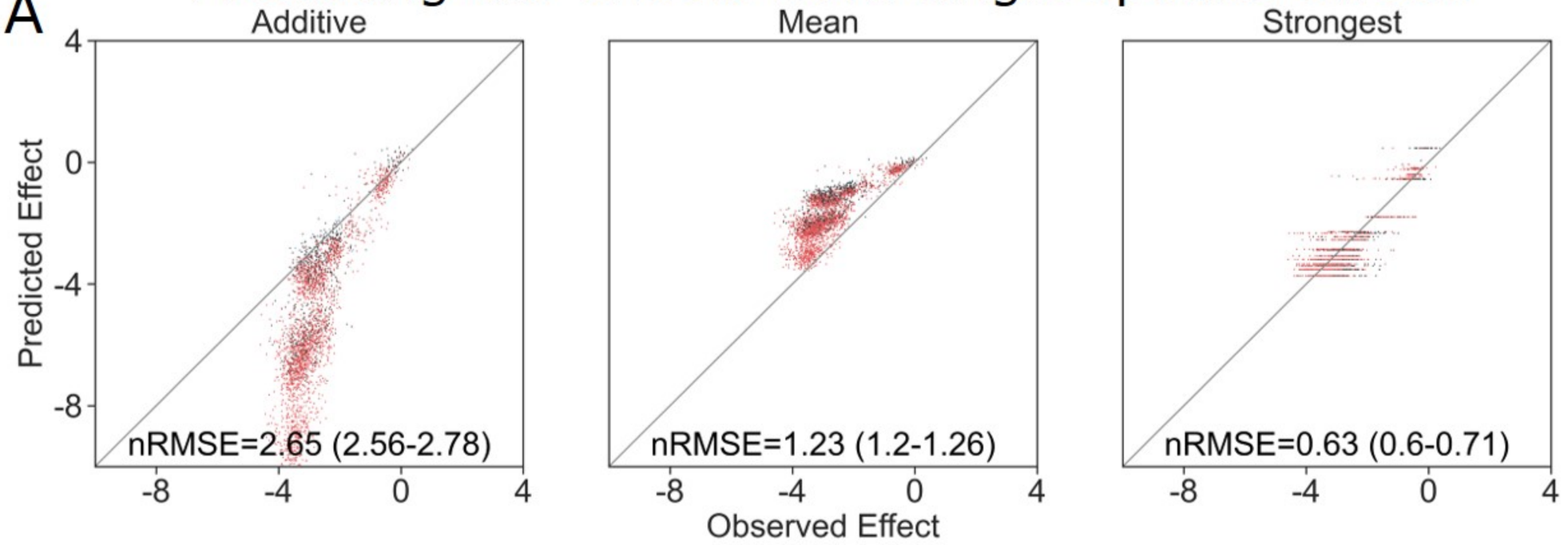

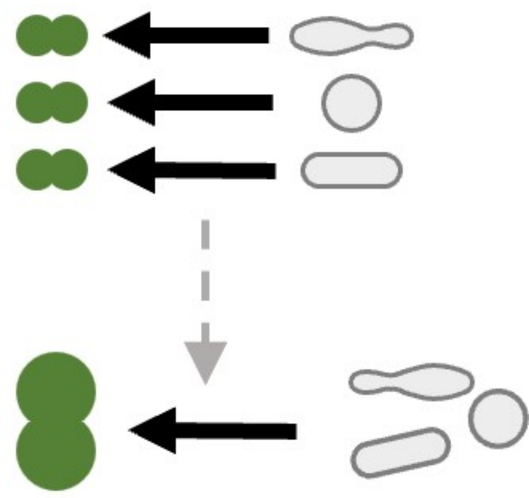

Predicting trio effects from pair effects

B

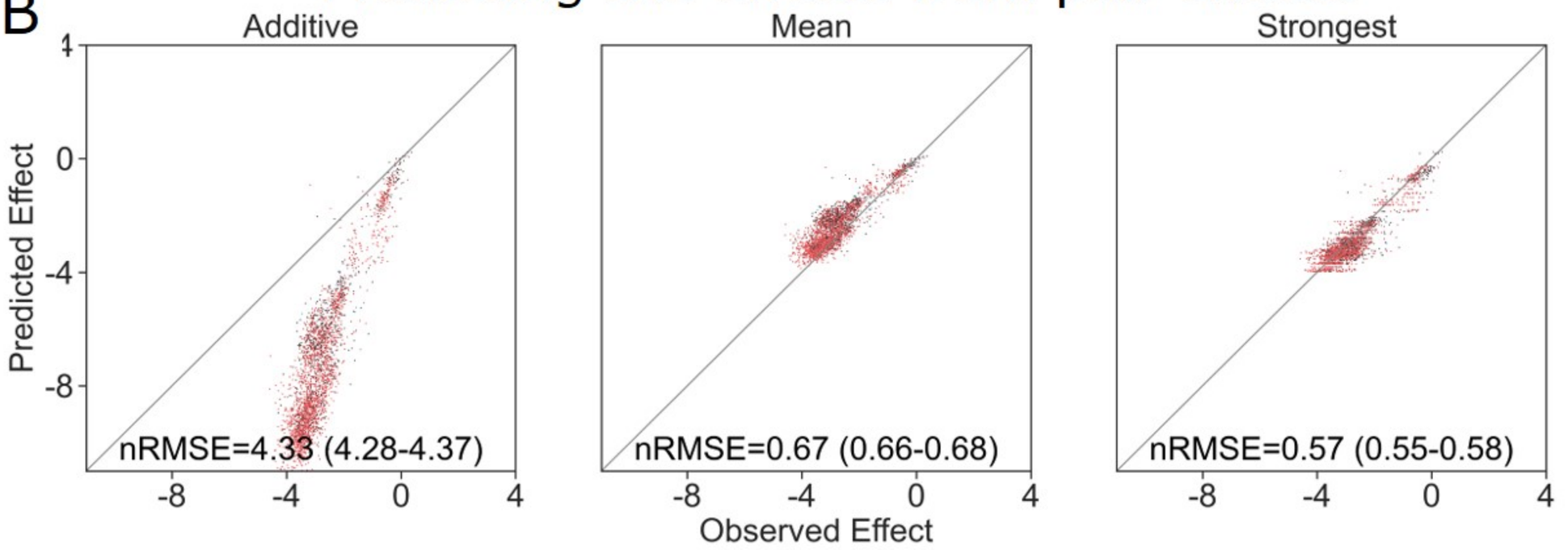

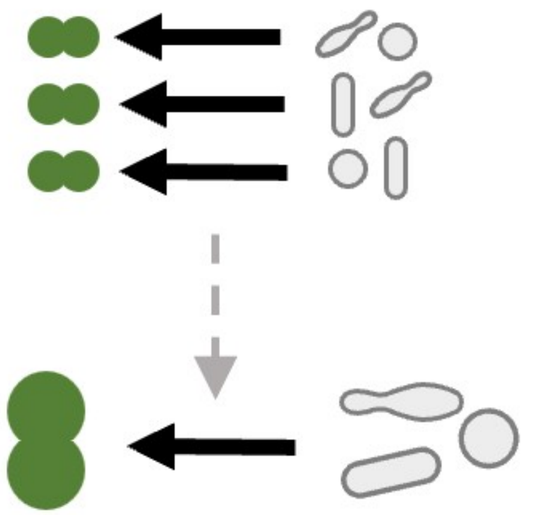

Distribution of effects and errors

C

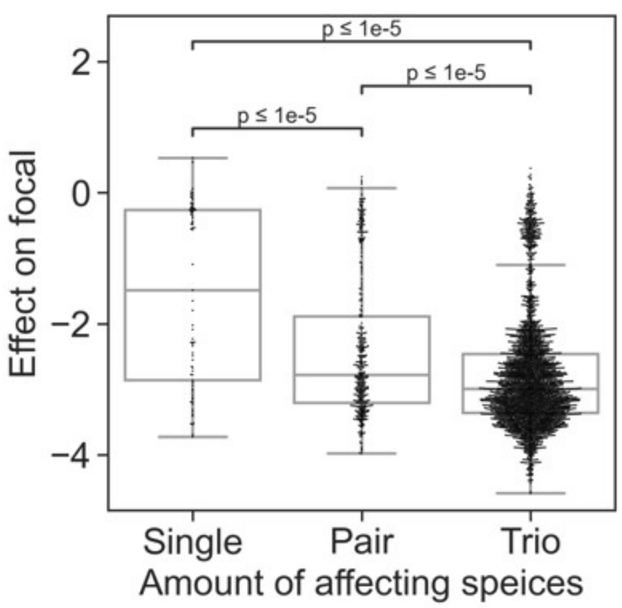

D

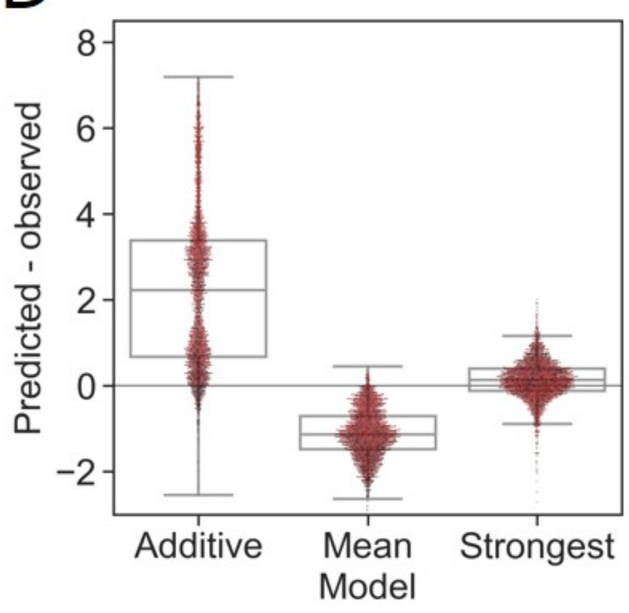

E

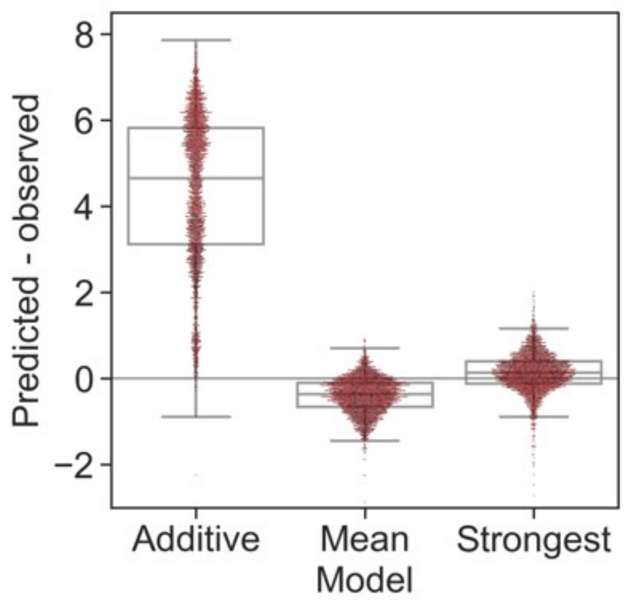

Qualitative single species effects

- Negative, Negative
- Negative, Positive
- Positive, Positive

Additive

Mean

OD Weighted

Strongest

Predicted Effect

Observed Effect

4

0

-4

-8

nRMSE=2.65 (2.56-2.78)

nRMSE=1.23 (1.2-1.26)

nRMSE=0.98 (0.97-1.0)

nRMSE=0.63 (0.6-0.71)

Sign of single species effects

Negative, Negative

Negative, Positive

Positive, Positive

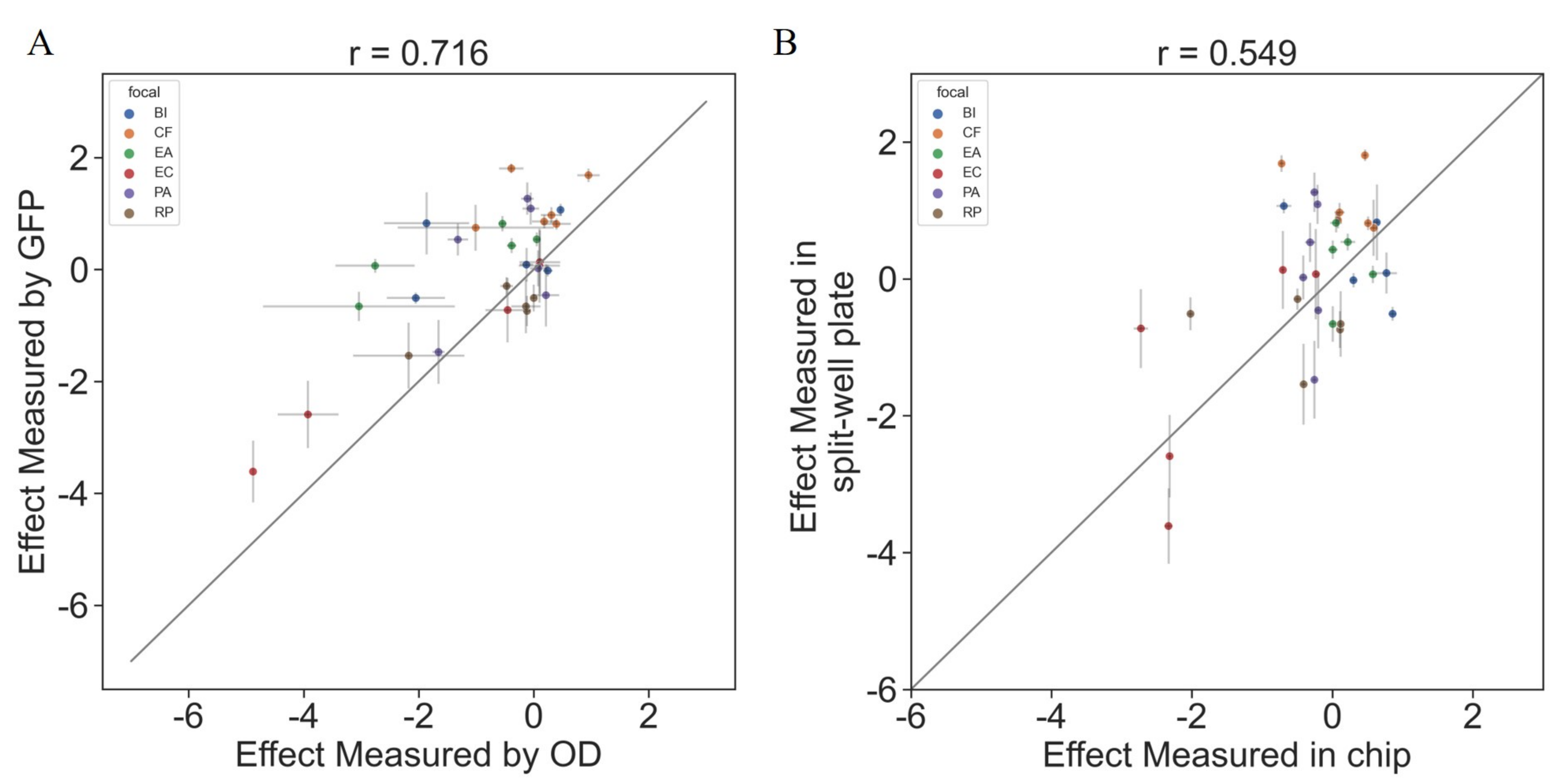
A
r = 0.716
focal
BI
CF
EA
EC
PA
RP
Effect Measured by GFP
Effect Measured by OD
2
0
-2
-4
-6
B
r = 0.549
Effect Measured in split-well plate
Effect Measured in chip

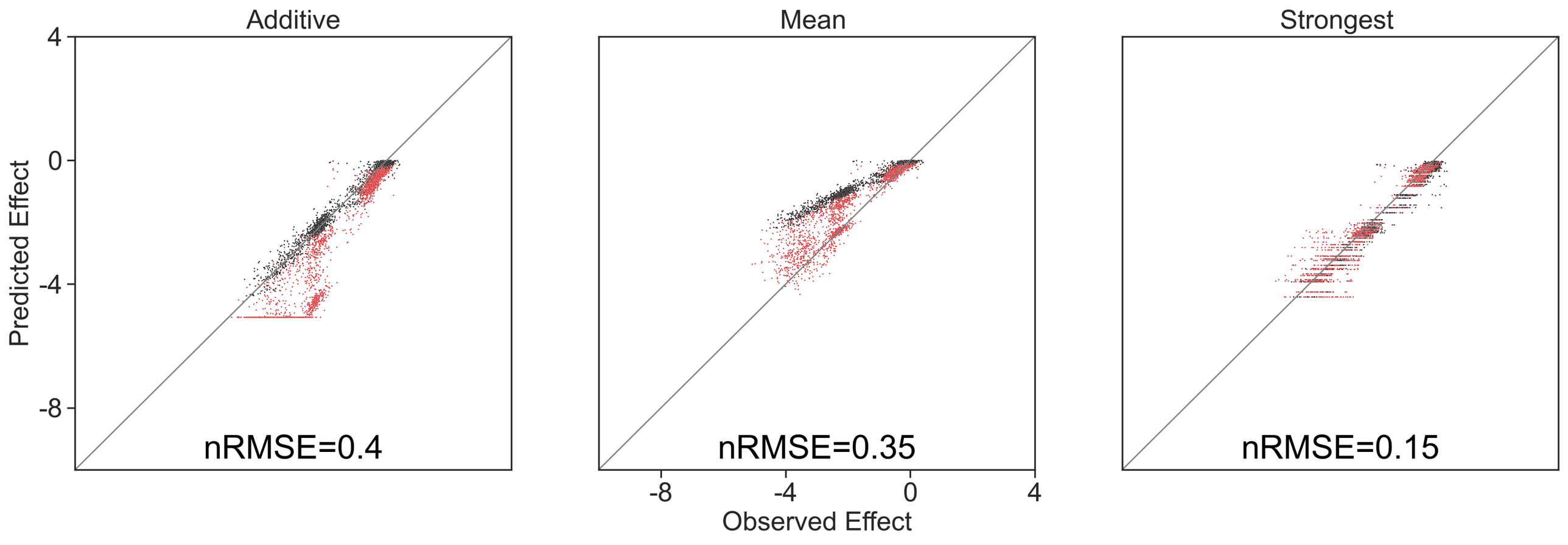
Additive
Mean
Strongest
Predicted Effect
Observed Effect
4
0
-4
-8
nRMSE=0.4
nRMSE=0.35
nRMSE=0.15

A

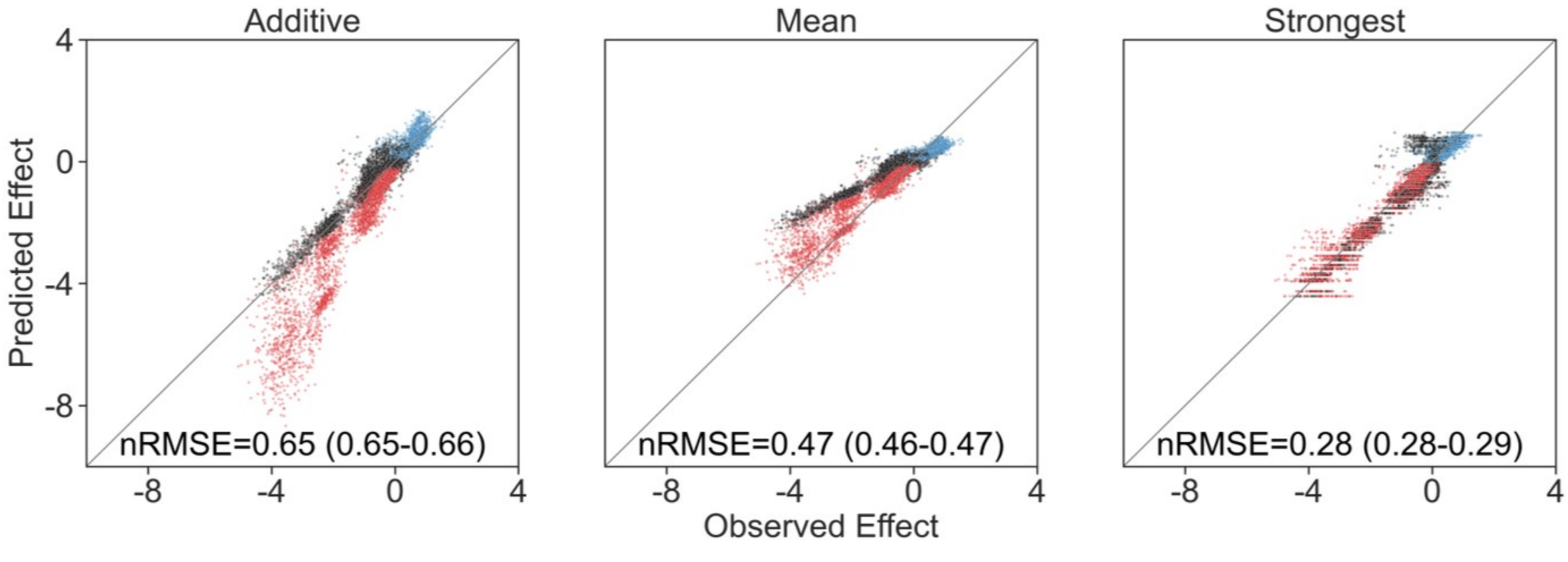
Predicting pair effects from single species effects
Additive
Mean
Strongest
Predicted Effect
Observed Effect
nRMSE=0.65 (0.65-0.66)
nRMSE=0.47 (0.46-0.47)
nRMSE=0.28 (0.28-0.29)
4
0
-4
-8

B

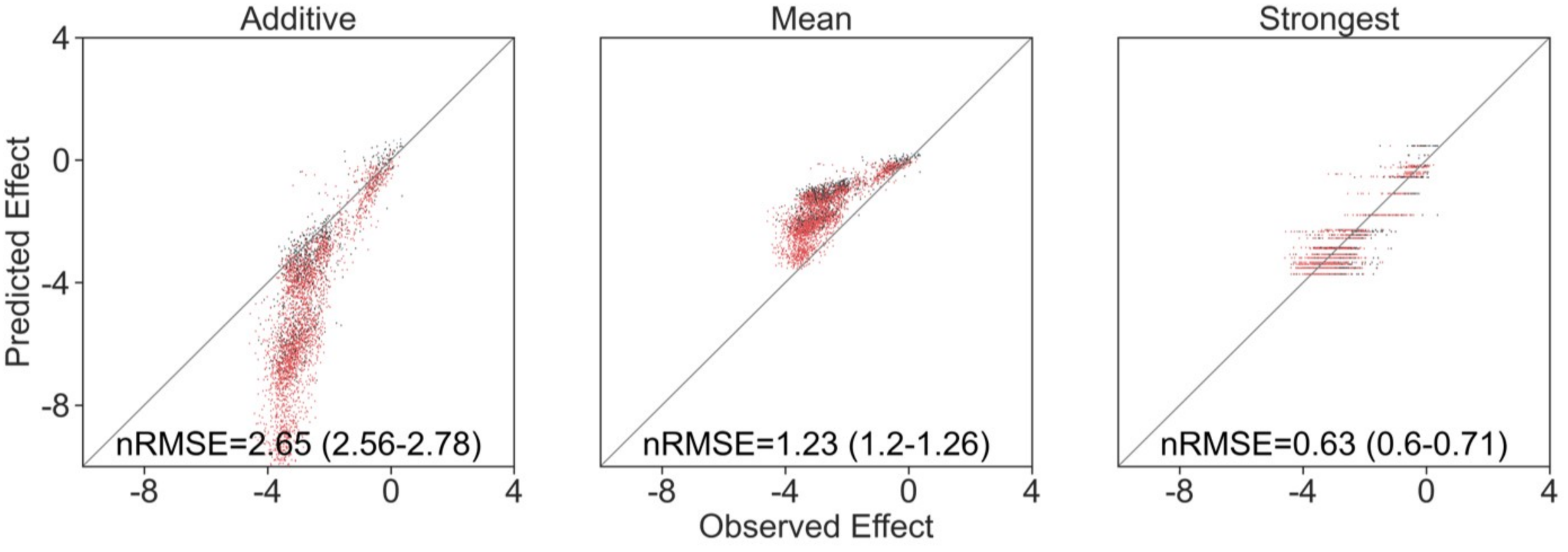
Predicting trio effects from single species effects
Additive
Mean
Strongest
Predicted Effect
Observed Effect
nRMSE=2.65 (2.56-2.78)
nRMSE=1.23 (1.2-1.26)
nRMSE=0.63 (0.6-0.71)
4
0
-4
-8

C

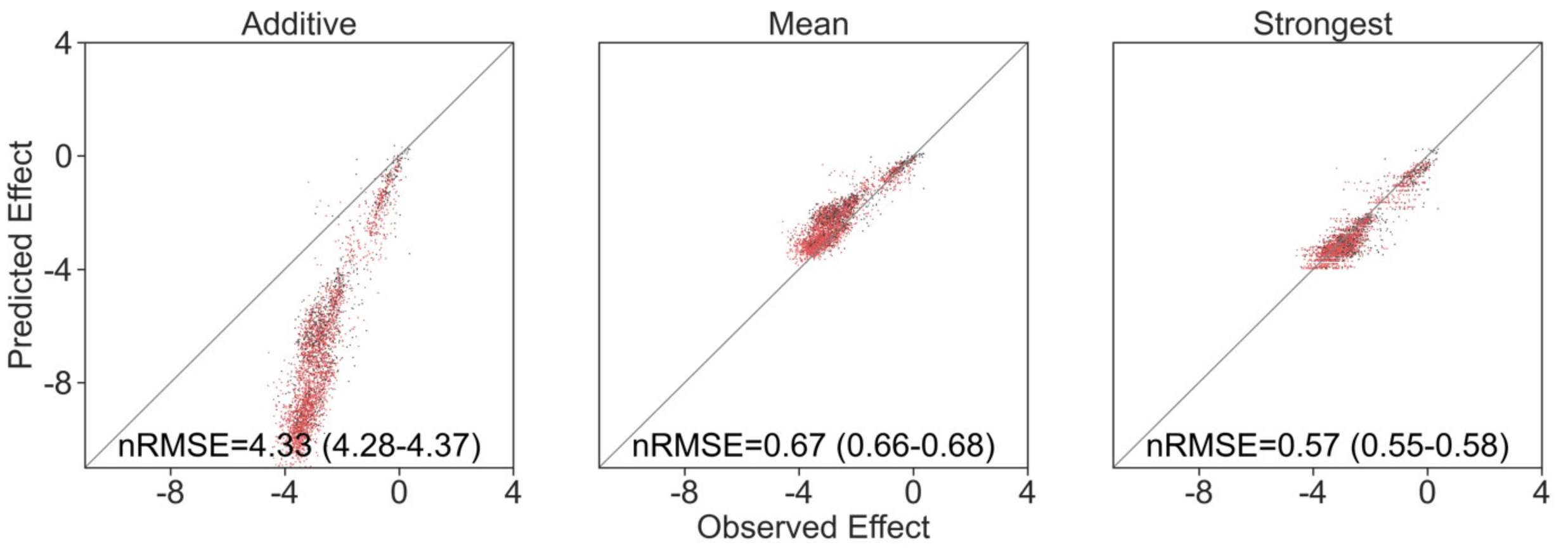
Predicting trio effects from pair effects
Additive
Mean
Strongest
Predicted Effect
Observed Effect
nRMSE=4.33 (4.28-4.37)
nRMSE=0.67 (0.66-0.68)
nRMSE=0.57 (0.55-0.58)
4
0
-4
-8